

AD-A257 631



②

NAVAL POSTGRADUATE SCHOOL

Monterey, California



S DTIC
ELECTE
DEC 01 1992 **D**
E

THESIS

FORCE OVERRIDE RATE CONTROLLER
FOR REMOTE ACTUATION

by

James M. Syvertsen

September, 1992

Thesis Advisor:

Morris R. Driels

Approved for public release; distribution is unlimited

92-30486

REPORT DOCUMENTATION PAGE				
1a. REPORT SECURITY CLASSIFICATION Unclassified		1b. RESTRICTIVE MARKINGS		
2a. SECURITY CLASSIFICATION AUTHORITY		3. DISTRIBUTION/AVAILABILITY OF REPORT Approved for public release; distribution is unlimited.		
2b. DECLASSIFICATION/DOWNGRADING SCHEDULE				
4. PERFORMING ORGANIZATION REPORT NUMBER(S)		5. MONITORING ORGANIZATION REPORT NUMBER(S)		
6a. NAME OF PERFORMING ORGANIZATION Naval Postgraduate School	6b. OFFICE SYMBOL (If applicable) 34	7a. NAME OF MONITORING ORGANIZATION Naval Postgraduate School		
6c. ADDRESS (City, State, and ZIP Code) Monterey, CA 93943-5000		7b. ADDRESS (City, State, and ZIP Code) Monterey, CA 93943-5000		
8a. NAME OF FUNDING/SPONSORING ORGANIZATION	8b. OFFICE SYMBOL (If applicable)	9. PROCUREMENT INSTRUMENT IDENTIFICATION NUMBER		
8c. ADDRESS (City, State, and ZIP Code)		10. SOURCE OF FUNDING NUMBERS		
		Program Element No.	Project No.	Task No. Work Unit Accession Number
11. TITLE (Include Security Classification) FORCE OVERRIDE RATE CONTROLLER FOR REMOTE ACTUATION				
12. PERSONAL AUTHOR(S) James M. Syvertsen				
13a. TYPE OF REPORT Master's Thesis	13b. TIME COVERED From To	14. DATE OF REPORT (year, month, day) September 1992	15. PAGE COUNT 80	
16. SUPPLEMENTARY NOTATION The views expressed in this thesis are those of the author and do not reflect the official policy or position of the Department of Defense or the U.S. Government.				
17. COSATI CODES		18. SUBJECT TERMS (continue on reverse if necessary and identify by block number)		
FIELD	GROUP	SUBGROUP		
19. ABSTRACT (continue on reverse if necessary and identify by block number) Many remotely operated robotic manipulator systems are operated in rate control mode to achieve a commanded position and orientation of the end-effector. Performance of certain tasks, such as applying a torque to a screw, would be more efficient if performed in unilateral force control mode. A six axis force-torque model was developed to determine the require number and positioning of sensors and using force sensing resistors, a prototype force-torque transducer was built for testing. Using a force error signal, individual joint angles may be computed in and algorithm to achieve force replication in the end-effector.				
20. DISTRIBUTION/AVAILABILITY OF ABSTRACT <input checked="" type="checkbox"/> UNCLASSIFIED/UNLIMITED <input type="checkbox"/> SAME AS REPORT <input type="checkbox"/> DTIC USERS		21. ABSTRACT SECURITY CLASSIFICATION Unclassified		
22a. NAME OF RESPONSIBLE INDIVIDUAL Driels, Morris R.		22b. TELEPHONE (Include Area code) (408)-646-3383	22c. OFFICE SYMBOL ME/Dr	

DD FORM 1473, 84 MAR

83 APR edition may be used until exhausted
All other editions are obsolete

SECURITY CLASSIFICATION OF THIS PAGE

Unclassified

Approved for public release; distribution is unlimited.

**FORCE OVERRIDE RATE CONTROLLER
FOR REMOTE ACTUATION**

by

**James Michael Syvertsen
Lieutenant, United States Navy
B.S., United States Naval Academy, 1985**

Submitted in partial fulfillment
of the requirements for the degree of

MASTER OF SCIENCE IN MECHANICAL ENGINEERING

from the


NAVAL POSTGRADUATE SCHOOL

September 1992

Author:


James M. Syvertsen

Approved by:


Morris Driels, Thesis Advisor


Matthew Kelleher, Chairman

Department of Mechanical Engineering

ABSTRACT

Many remotely operated robotic manipulator systems are operated in rate control mode to achieve a commanded position and orientation of the end-effector. Performance of certain tasks, such as applying a torque to a screw, would be more efficient if performed in unilateral force control mode. A six axis force-torque model was developed to determine the required number and positioning of sensors and using force sensing resistors, a prototype force-torque transducer was built for testing. Using a force error signal, individual manipulator joint angles may be computed in an algorithm to achieve force replication in the end-effector.

Accession For	
NTIS	CRA&I <input checked="" type="checkbox"/>
DTIC	TAB <input type="checkbox"/>
Unannounced <input type="checkbox"/>	
Justification	
By	
Distribution /	
Availability Codes	
Dist	Avail and/or Special
A-1	

TABLE OF CONTENTS

I. INTRODUCTION	1
II. PRELIMINARY WORK	4
A. FORCE OVERRIDE RATE CONTROLLER	4
1. Objectives	4
2. Background	4
3. Technical Approach	5
4. Control Analysis	8
5. Simulation and Testing	11
III. SENSOR DEVELOPMENT	13
A. THEORY	13
1. Force Sensing	13
2. Force Sensing Resistors	15
3. Transducer Design	16
a. Preliminary Design	16
b. Sensor Placement	17
4. Development of Sensor Equations	19
5. Sensor Placement	21
a. Methodology	21
b. Transducer Design Optimization	29
c. Reduced Order Transducer	31

B.	PROTOTYPE TRANSDUCER DESIGN	34
1.	Mechanical Design	34
2.	Transducer Testing and Calibration	37
IV.	FORCE CONTROL	39
A.	THEORY	39
1.	Robotic Application of Transducer	39
2.	Manipulator Kinematics	39
a.	Generalized Coordinate Transformations	39
b.	Compound Transformations	41
c.	Denavit-Hartenberg Transformations	43
d.	PUMA 560 Denavit-Hartenberg Parameters	46
e.	PUMA 560 Forward Kinematics	48
f.	Inverse Manipulator Kinematics	49
3.	Jacobian Development	51
a.	Static Forces in Manipulators	51
b.	Manipulator Jacobian in the Force Domain	53
B.	IMPLEMENTATION	54
1.	Force Override Rate Controller Algorithm	54
V.	CONCLUSIONS	55
A.	EXPERIMENTAL AND THEORETICAL RESULTS	55
B.	FURTHER WORK	55
	APPENDIX A	56

APPENDIX B	61
APPENDIX C	64
LIST OF REFERENCES	67
INITIAL DISTRIBUTION LIST	69

LIST OF TABLES

TABLE 1.	ASSUMED GAIN CONSTANTS12
TABLE 2.	BIPLANAR TRANSDUCER COEFFICIENT ARRAY . . .	23
TABLE 3.	SIX AXIS TRANSDUCER COEFFICIENT ARRAY . . .	26
TABLE 4.	PROTOTYPE TRANSDUCER WIRING CODE35
TABLE 5.	OPERABLE SENSOR COEFFICIENT ARRAY37
TABLE 6.	PUMA 560 LINK AND JOINT PARAMETERS47
TABLE 7.	54 SENSOR COEFFICIENT ARRAY56
TABLE 8.	SENSOR ELIMINATION STRATEGY58
TABLE 9.	24 SENSOR COEFFICIENT ARRAY59
TABLE 10.	SENSOR ELIMINATION STRATEGY60

LIST OF FIGURES

Figure 1.	PUMA 560 Manipulator Washing a Window . . .	2
Figure 2.	Wrist Mounted Force/Torque Sensor	5
Figure 3.	Single DOF Hydraulic Actuation System . . .	6
Figure 4.	Force Override Rate Control Loop	8
Figure 5.	Controller Block Diagram	9
Figure 6.	Modified Controller Block Diagram	11
Figure 7.	Controller Response to Step Input	12
Figure 8.	FSR and Characteristics	16
Figure 9.	FSR-Based Transducer Conceptual Design . . .	17
Figure 10.	Planar Joystick	20
Figure 11.	Transducer with 8 Sensors	22
Figure 12.	Six Axis Transducer	25
Figure 13.	54 Sensor Transducer	27
Figure 14.	Optimized Full Order Transducer	30
Figure 15.	Reduced Order Transducer	33
Figure 16.	Prototype Transducer Mechanical Design . . .	36
Figure 17.	Robotic Application of Transducer	40
Figure 18.	Translated and Rotated Link Frame	42
Figure 19.	Generic Manipulator Link	45
Figure 20.	PUMA Link Frame Assignments	47
Figure 21.	Forces on a Manipulator Link	51
Figure 22.	Force Control Algorithm	54

ACKNOWLEDGMENT

I wish to express my appreciation to NASA for their sponsorship and funding of this project, to the Naval Postgraduate School for the opportunity to further my knowledge of engineering, and to Professor Morris Driels for his patience and understanding, and allowing me the privilege of working with him on this project. Also, I wish to extend a special note of thanks to Jim Schofield, Tom Christian and the Machine Shop for their patience and technical help in building and testing the prototype transducer.

I. INTRODUCTION

The main objective addressed in this thesis is the design and implementation of a transducer and control system for a manipulator which allows force control to override the normal mode of rate control. For a manipulator operating in free space, rate control is sufficient for most tasks. Use of a force/torque sensor mounted in the wrist frame of a manipulator arm allows an operator to perform certain tasks in which contact forces develop. There are, however, inherent limitations in reliance on a position sensing based controller as a result of the repeatability and accuracy constraints of any manipulator system. While it is certainly within our technical capability to develop more accurate sensing systems and build more precise manipulators, the cost may very well be prohibitive relative to the utility. It would be far more practical and efficient to develop a means by which to **measure and control contact forces**.

For assembly tasks such as the mating of two parts or applying a specific torque to a screw, rate control does not suffice. A simple example of the utility of force control is illustrated in Figure 1 which shows the *PUMA 560 Manipulator* washing a window. If this task were performed under rate control, positional uncertainty may result in the window being

broken. It would be far more reasonable to specify a force to be maintained normal to the surface of the glass.

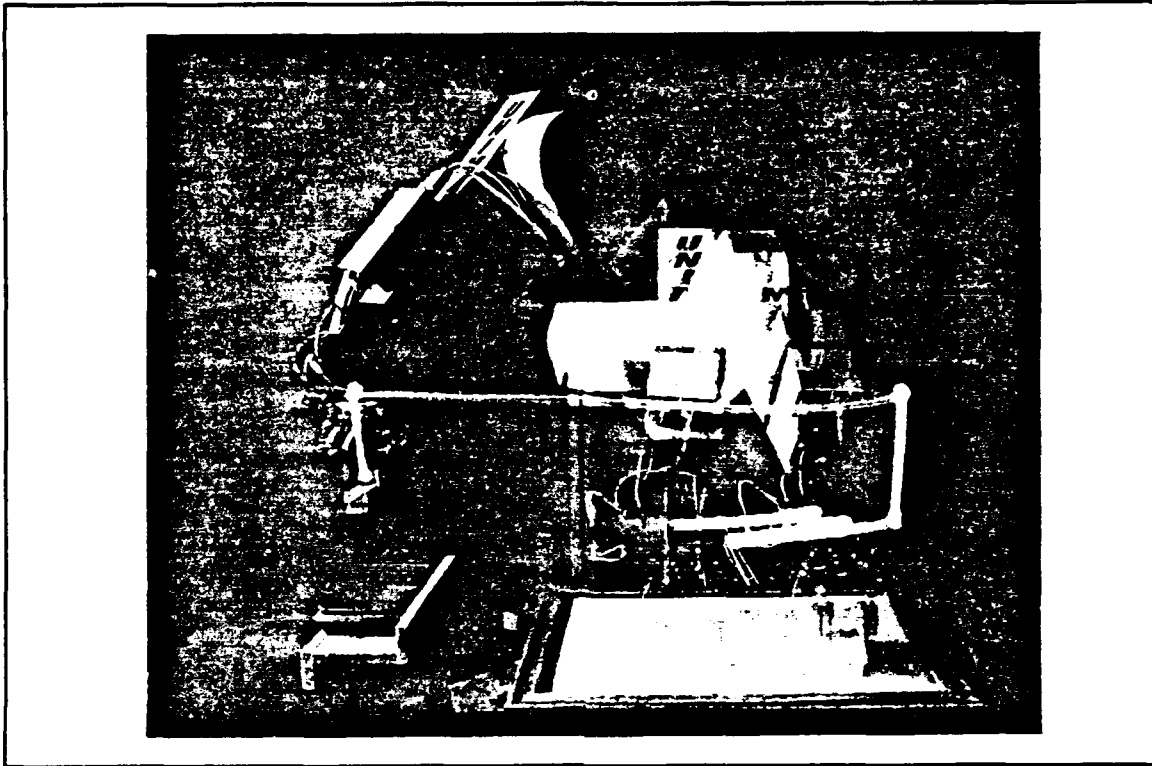


Figure 1. PUMA 560 Manipulator Washing a Window [Ref. 1]

Although force-torque transducers have already been developed using strain gauges, there is a relatively new technology, known as the **Force Sensing Resistor™** (FSR), which has already been implemented in applications using human touch as an input. Successful implementation of an *FSR-based force-torque transducer* would prove to be a far more cost effective, electronically simplified and robust means of measuring and controlling contact forces than the strain gauge-based transducers currently in use. Furthermore, the *FSR* represents a vibrant new technology with a host of space related

applications such as the **Space Shuttle Manipulator Arm**. Development of a transducer using this technology and a proposed method for implementation in a force override rate controller are presented.

II. PRELIMINARY WORK

A. FORCE OVERRIDE RATE CONTROLLER

1. Objectives

The purpose of the project was to design and prototype a control system for a remote actuator such as a robotic manipulator arm to allow force control to override the normal rate control governing movement of the manipulator.

2. Background

Manipulator systems such as the *Space Shuttle RMS* are often operated remotely in rate control mode in which a constant controller input, such as a fixed angular displacement of a joystick for example, produces a constant tip velocity along the trajectory of the manipulator. When the end-effector encounters a rigid object, however, further actuation is nullified when the sensed force exceeds an operator specified threshold. The Shuttle RMS operates in this manner utilizing a six axis force-torque sensor similar to the model depicted in Figure 2.

The shortcomings of a position sensing based controller may be overcome through the use of a hybrid position/force control scheme in which the "shoulder" and "elbow" joints are controlled with a position controller and the "wrist" joints controlled with a force controller. While

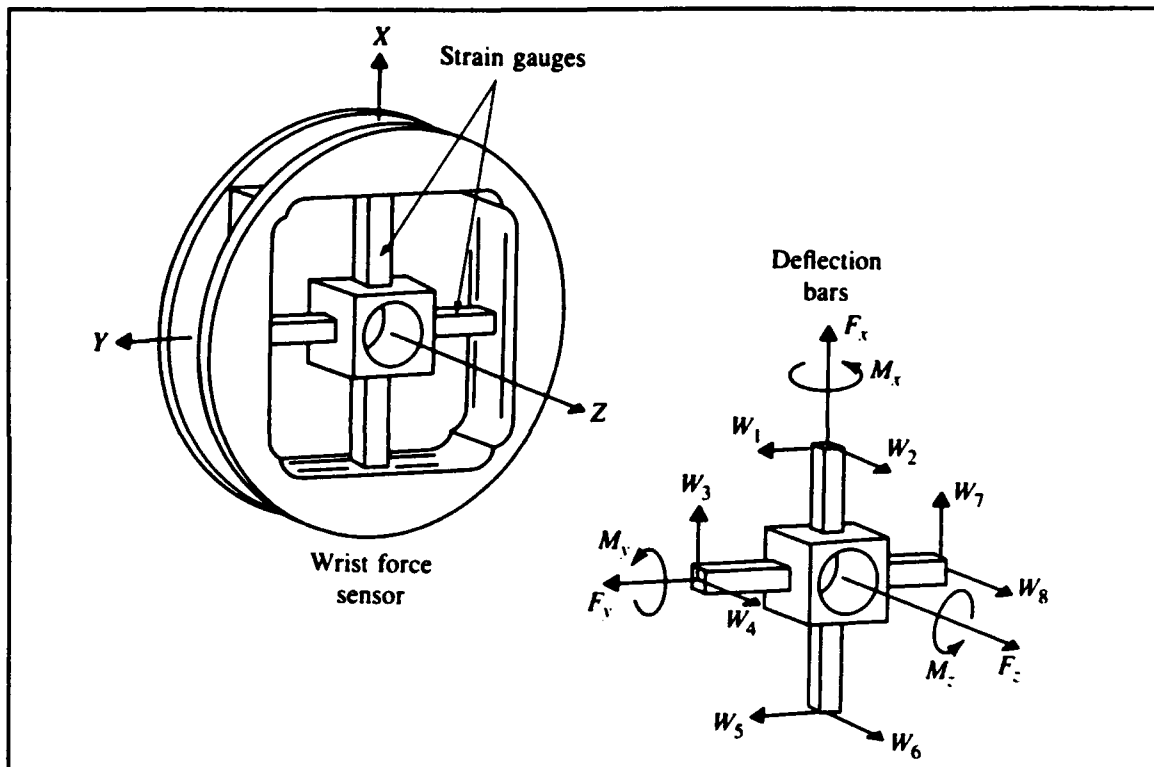


Figure 2. Wrist Mounted Force/Torque Sensor [Ref. 2]

seemingly the ideal solution, the hybrid controller must be capable of implementing and mixing the position and force control modes and may become quite cumbersome. It would be more convenient as well as more efficient if the individual joints could be operated in unilateral force control mode so that operator applied forces could be reflected at the manipulator tip. The following section illustrates in simple fashion the implementation of a remotely actuated force controller.

3. Technical Approach

To demonstrate the basic approach, consider the one degree of freedom actuation system depicted in Figure 3. In

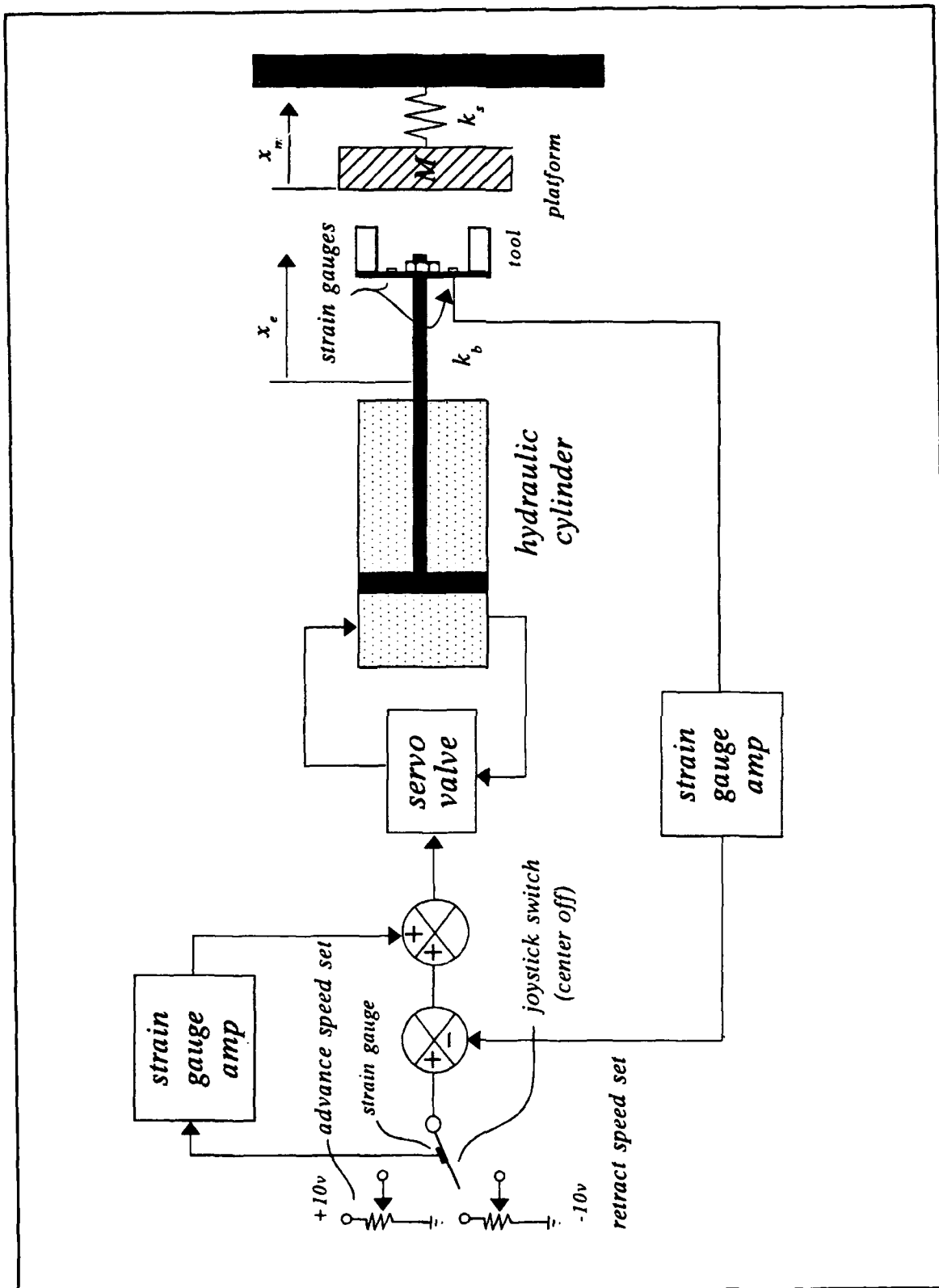


Figure 3. Single DOF Hydraulic Actuation System

response to an angular displacement of the joystick, the servo valve allows hydraulic fluid to flow to/from the hydraulic cylinder, thus controlling the velocity of the ram. Force sensing is accomplished by means of strain gauges or force sensing resistors (FSR) mounted on the tool. The spring attached to the mass is used in the control loop to simulate compliance of the external constraint.

Control of this actuation system is illustrated by the simple control loop in Figure 4 in which the open switch represents the joystick in the vertical position. The quantity F_d is a force threshold set by the operator using a potentiometer at which control shifts from rate mode to the force control mode. When the joystick is displaced by some angle β , the switch is closed and a voltage command is supplied to the actuator causing the tool to move with velocity \dot{x} until the tool comes in contact with the mass-spring. Actuator movement ceases when the measured force signal is equal to F_d . If additional force is applied to the joystick the force sensors mounted on the stick increase the forward path signal causing further motion of the hydraulic ram and increasing the force applied to the external constraint by the tool. Thus the operator has the capability to reflect forces applied to the joystick at the tip of the actuation system in a proportional manner.

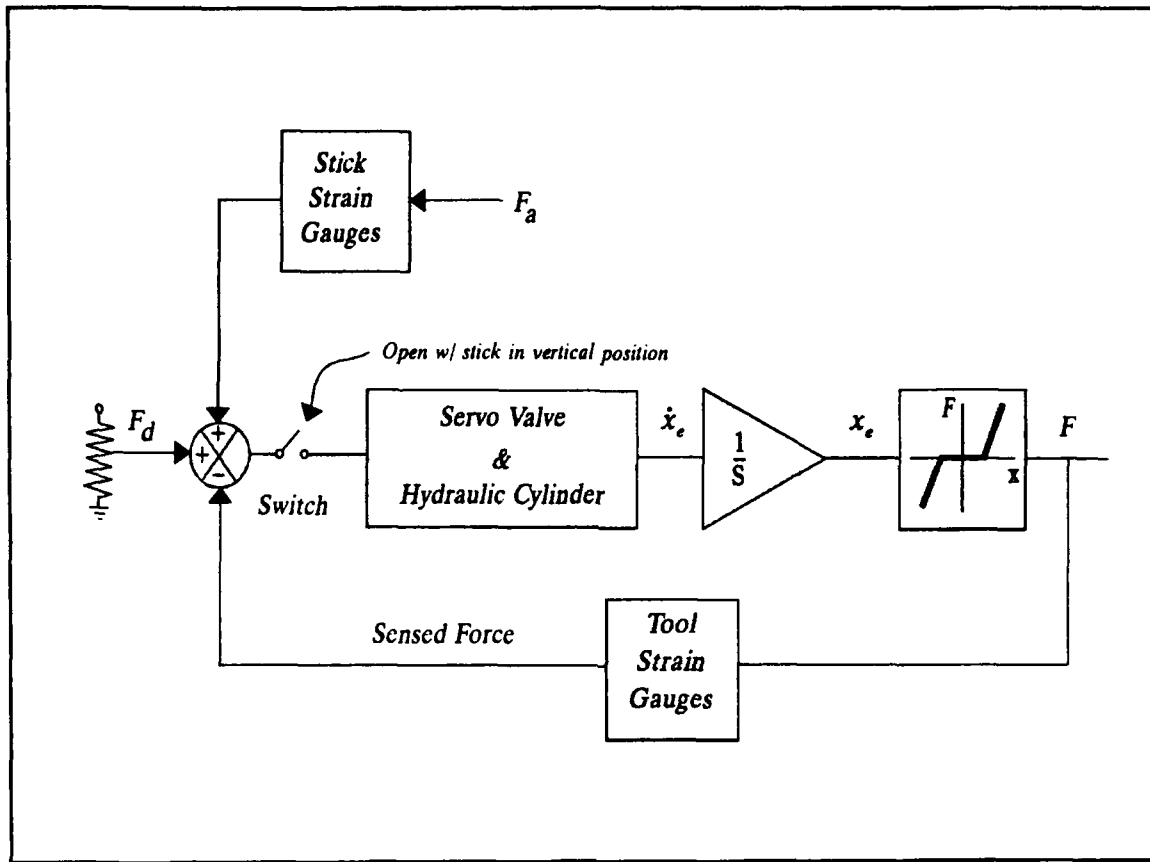


Figure 4. Force Override Rate Control Loop

4. Control Analysis

This system may be modelled by the block diagram in Figure 5 for computer simulation where k_s represents the servo gain and k_a the actuator gain; x_e is the linear position of the tip of the tool with respect to some reference frame and x_m is the linear deflection of the mass-spring. The gain k_x is a stiffness ratio relating the stiffnesses of the mass-spring and the tool. Summing forces yields the following equation:

$$-\Sigma F_x = k_b(x_e - x_m) - k_s x_m = 0 \quad (1)$$

Manipulation of Equation (1) results in the following

$$x_m = \frac{k_b}{(k_b + k_g)} x_e \quad (k_b > k_g) \quad (2)$$

where k_b denotes the tool stiffness and the ratio of spring constants is defined as the stiffness ratio k_x . The transfer function that appears in the forward path is an electronic first order servo lag with selectable time constant τ . The gain constant denoted by k_g is a feedback transfer function relating the displacement of the end-effector and the voltage output for strain gauge amplifiers.

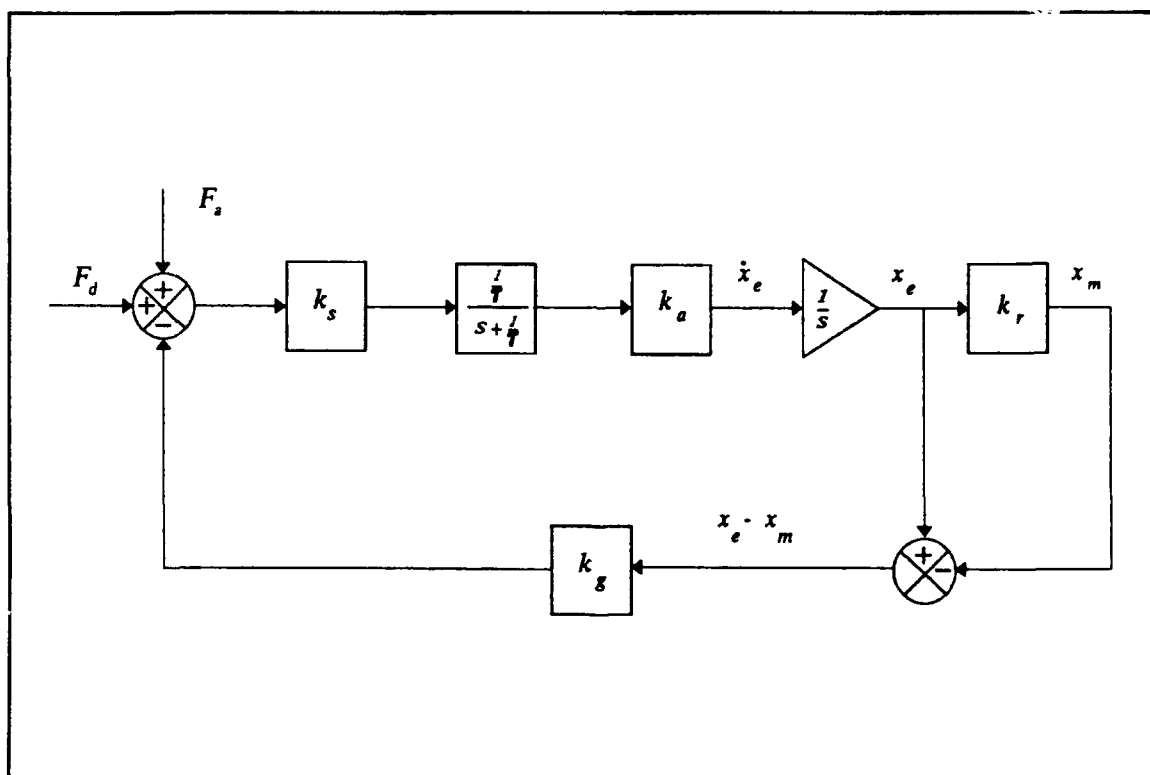


Figure 5. Controller Block Diagram

The block diagram in Figure 5 may be simplified by performing a few simple block diagram algebraic operations.

$$\Delta x = x_e - x_m \quad (3)$$

$$x_m = k_r x_e \quad (4)$$

Substituting Equation (4) into (3)

$$\Delta x = x_e - k_r x_e = x_e(1 - k_r) \quad (5)$$

Using Equation (5), the second summing junction may be eliminated and the block diagram modified to the simpler form in Figure 6, where the output and the closed loop transfer function are given by Equations (6) and (7) respectively.

$$x_e(s) = \frac{G(s)}{1 + GH(s)} F(s) \quad (6)$$

$$\frac{x_e}{F} = \frac{\frac{1}{\tau} k_s k_a}{s^2 + \frac{1}{\tau} s + \frac{1}{\tau} k_s k_a k_g (1 - k_r)} \quad (7)$$

The denominator portion of Equation (7) represents the characteristic equation for the system, indicating a second order system of the form

$$s^2 + 2\xi\omega_n s + \omega_n^2 \quad (8)$$

where

$$\omega_n^2 = \frac{1}{\tau} k_s k_a k_g (1 - k_r) \quad (9)$$

and the damping ratio is

$$\xi = \frac{1}{(2\omega_n\tau)} \quad (10)$$

The actuator gain and stiffness ratio denoted by k_a and k_s respectively are fixed values. The servo gain, k_s and the feedback transfer function gain, k_g are variables and their optimal values may be determined by the *pole placement method*.

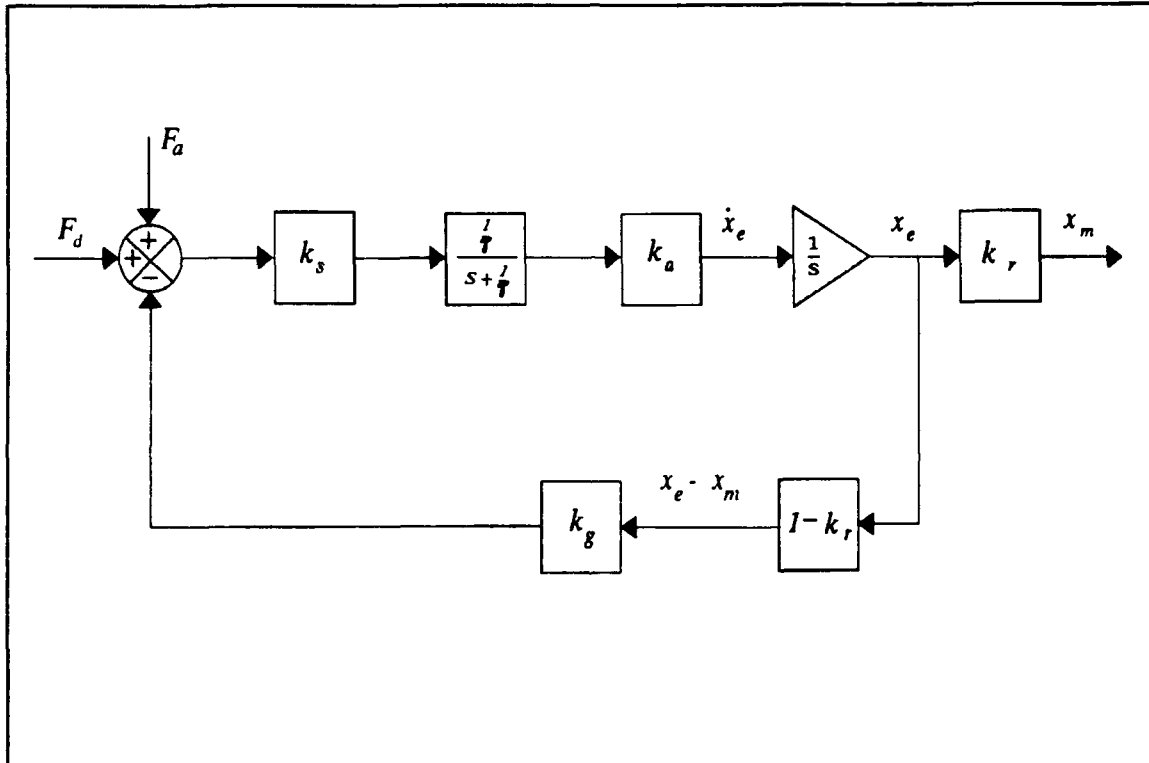


Figure 6. Modified Controller Block Diagram

5. Simulation and Testing

Using the results of the previous section, operational performance was simulated using *MATRIXx* and *MATLAB*. A unit step function was used to simulate the joystick input and a nominal value of 0.1 was selected for the time constant τ . The

following table gives the assumed values for the gain constants. Using these values, the simulated response was characteristic of a second order system as depicted in Figure 7 and observed in experimental testing. The result was confirmed in tests using the *PUMA 560 Manipulator*.

TABLE 1. Assumed Gain Constants

Name	Symbol	Value
Servo Gain	k_s	15 v/v
Actuator Gain	k_a	2 m/s/v
Stiffness Ratio	k_r	0.9 v/m
Feedback T.F. Gain	k_g	2

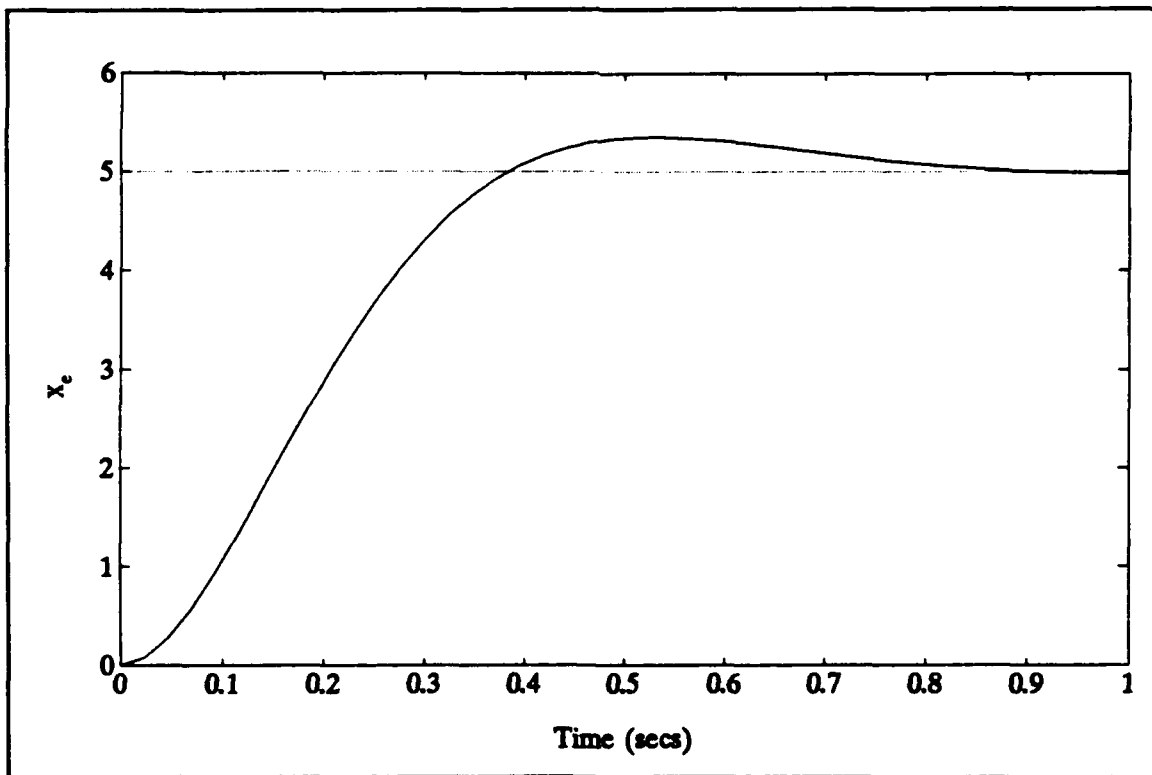


Figure 7. Controller Response to Step Input

III. SENSOR DEVELOPMENT

A. THEORY

1. Force Sensing

Many operations performed by a robot manipulator arm require some means of force sensing capability. Some type of force-torque sensor is typically mounted in the wrist frame between the tip of the manipulator arm and the end-effector. For a robot arm that is tasked with gripping and transporting fragile objects or washing a window for example, the ability of the robot to sense the applied force is critical in nature. Most wrist sensors "sense" forces and torques applied at the end effector by transforming the applied forces/moments into measurable deflections or displacements. The wrist sensor depicted in Figure 2 uses eight pairs of strain gauges wired to a potentiometer circuit to determine three components of force F and three moment components M by producing output voltages proportional to the applied force/moment. Premultiplying this sensor data matrix by the resolved force matrix produces three orthogonal force and three torque components. This assumes that all forces/moments can be decoupled, that strain gauge readings vary linearly for the applied force, and that temperature effects are negligible. As described by Fu [Ref. 3], eight voltage readings result from

elongation of the strain gauges. The force vector is determined from

$$F = R_F W \quad (11)$$

where

$$F \equiv (\text{forces, moments})^T = (F_x, F_y, F_z, M_x, M_y, M_z)^T$$

$$W \equiv \text{raw readings} = (w_1, w_2, w_3, \dots, w_8)^T$$

and

$$R_F = \begin{bmatrix} I_{11} & I_{12} & I_{13} & \cdot & I_{18} \\ I_{21} & \cdot & \cdot & \cdot & \cdot \\ I_{31} & \cdot & \cdot & \cdot & \cdot \\ \cdot & \cdot & \cdot & \cdot & \cdot \\ I_{61} & \cdot & \cdot & \cdot & I_{68} \end{bmatrix} \quad (12)$$

The non-zero elements of the R_F matrix are conversion factors to convert voltages to units of force or torque. In reality, it is highly likely that some coupling will exist and none of the 48 elements will be zero. Thus, in order to eliminate any existing coupling and obtain accurate force/moment readings, the force matrix must be calibrated such that

$$W = R_F^{cal} F \quad (13)$$

and

$$R_F^{cal} R_F = I_8 \quad (14)$$

where I_8 is an identity matrix and the calibration matrix is found by applying known weights along the axes of the sensor coordinate frame. Because R_F is a non-square matrix it is

necessary to utilize the **pseudoinverse**. Premultiplying a non-square matrix by its transpose produces a square matrix which if it is full rank, may then be inverted such that

$$F = [(R_F^{cal})^T R_F^{cal}]^{-1} (R_F^{cal})^T W \quad (15)$$

2. Force Sensing Resistors

Though strain gauges have been successfully applied in the design of wrist force sensors (or transducers), there are disadvantages to using them, the principle ones being the requirement for the part on which they are mounted to be capable of deflecting, precise interface electronics and relatively high cost.

The **Force Sensing Resistor™** (FSR) though not as accurate as strain gauges, are more rugged, significantly less expensive on a per unit cost basis and simple in design. They are thin (on the order of 0.008 to 0.030 inches) and composed of a semi-conducting polymer and conductive fingers sandwiched between two sheets of polymer (Figure 8a). Because of their purely resistive impedance, interface electronics are simplified. These devices have no moving parts and exhibit a decrease in resistance with increasing normal force applied to the active surface as shown in Figure 8b. Additional characteristics include a large dynamic range (1k Ω to 10M Ω), insensitivity to vibration, temperature, chemical and moisture resistance. The FSR is also not susceptible to hysteresis.

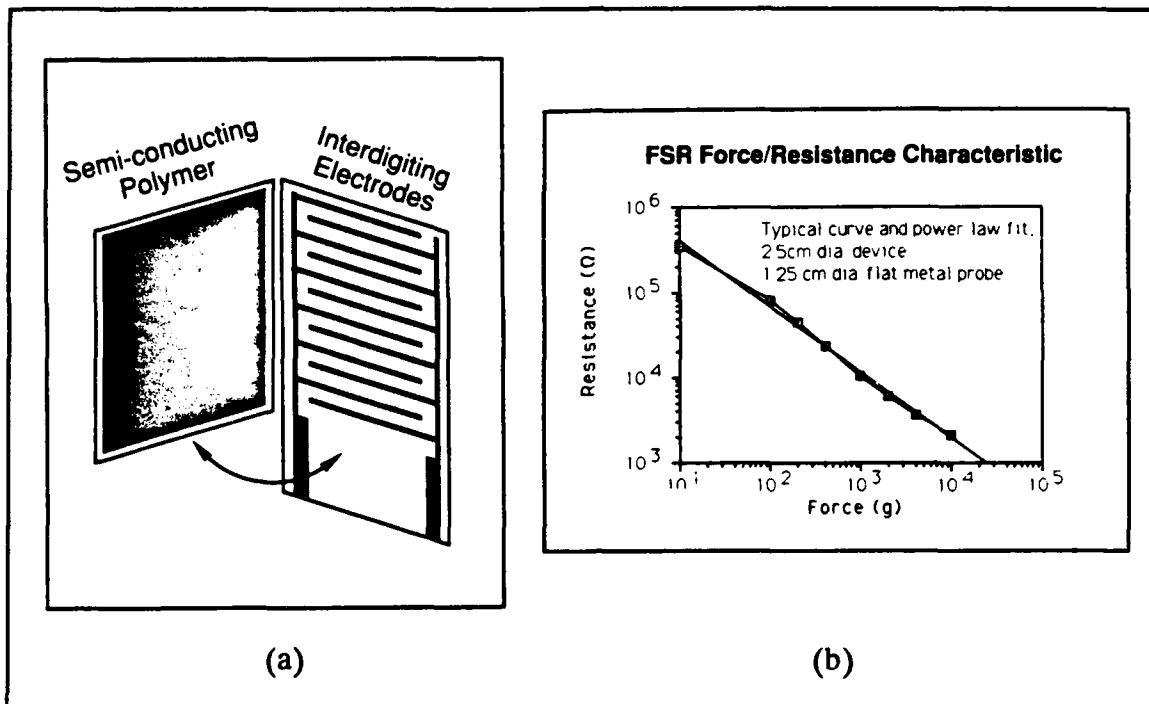


Figure 8. FSR and Characteristics [Ref. 4]

Though not suited for precision measurement, implementation of *FSRTM* technology into a manipulator force-torque transducer presents the opportunity for a more robust, less expensive and electronically simplified sensor.

3. Transducer Design

a. Preliminary Design

After suggesting an investigation into the feasibility of *FSR* application, the project sponsor at NASA proposed a conceptual design in which individual sensors are mounted on a cube which is then embedded in a semi-compliant material like RTV. Figure 9 illustrates the preliminary design that served as the conceptual basis on which transducer development proceeded.

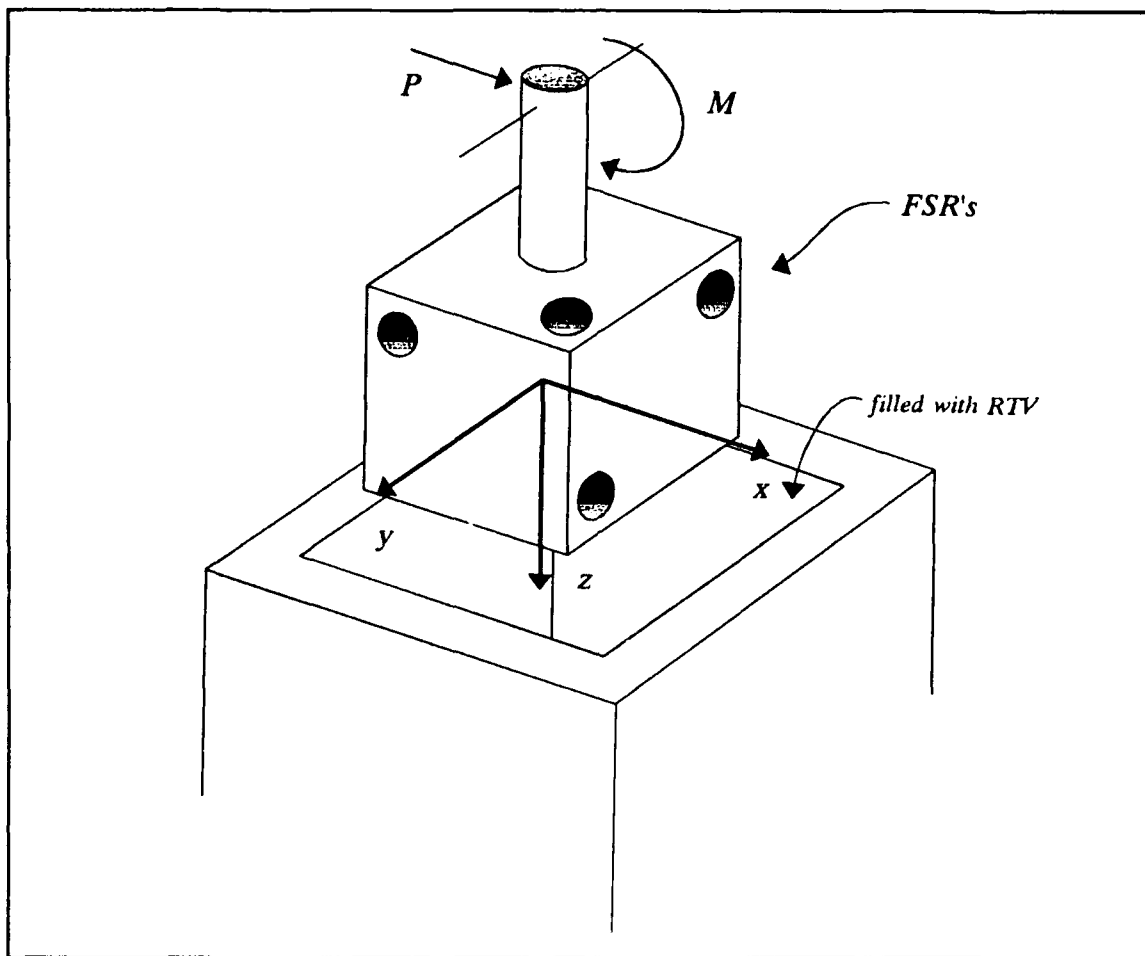


Figure 9. FSR-Based Transducer Conceptual Design

b. Sensor Placement

The first question that needed to be addressed was the placement of sensors. Assuming the sensors are mounted on an aluminum cube, how many sensors are required to be able to detect six force components (positive and negative) and six moments? Mathematically, the problem may be generalized using a matrix equation in the form of Equation (16)

$$\begin{vmatrix} S_1 \\ S_2 \\ \cdot \\ \cdot \\ \cdot \\ S_n \end{vmatrix} = \begin{vmatrix} a_{11} & a_{12} & a_{13} & \cdot & \cdot & \cdot & a_{112} \\ \cdot & a_{22} & \cdot & \cdot & \cdot & \cdot & \cdot \\ \cdot & \cdot & \cdot & \cdot & \cdot & \cdot & \cdot \\ \cdot & \cdot & \cdot & \cdot & \cdot & \cdot & \cdot \\ \cdot & \cdot & \cdot & \cdot & \cdot & \cdot & \cdot \\ a_{n1} & \cdot & \cdot & \cdot & \cdot & \cdot & a_{n12} \end{vmatrix} \begin{vmatrix} F_x^+ \\ F_x^- \\ F_y^+ \\ F_y^- \\ F_z^+ \\ F_z^- \\ M_x^+ \\ M_x^- \\ M_y^+ \\ M_y^- \\ M_z^+ \\ M_z^- \end{vmatrix} \quad (16)$$

where \mathbf{S} is an $n \times 1$ sensor output matrix and \mathbf{A} an $n \times 12$ sensor coefficient matrix. Because the FSR only responds to a compressive force, sensors must be strategically located to determine both positive and negative force/torque components. Hence, \mathbf{F} is a 12×1 force-torque component matrix. The question is: what is n and how are the sensors placed so that all force components and moments may be identified? To utilize the pseudoinverse, the matrix algebra dictates that the number of sensors must be greater than or equal to the number of force/torque components to be determined. If n is 12 then the force components may be determined from

$$\mathbf{F} = \mathbf{A}^{-1} \mathbf{S} \quad (17)$$

If the number of sensors is greater than twelve then \mathbf{A} cannot be inverted by itself being non-square. Premultiplying both

sides of Equation (16) by A^T produces a square matrix $A^T A$. If this matrix is full rank it may be inverted so that

$$F = (A^T A)^{-1} A^T S \quad (18)$$

Rank deficiency of this matrix implies that all components of F are not identifiable. The basic problem then is one of determining the minimum number of sensors required to detect all force/moment components and to determine where on the cube these sensors need to be placed to identify all force/moment components.

4. Development of Sensor Equations

Initial analysis was performed by modelling the sensor-transmitter as a planar joystick attached by springs to a rigid surface. Using the *principle of superposition*, equations were developed for each of the sensors to determine which sensors are activated when a particular force or moment is applied. Referring to Figure 10, the force applied to sensor number one for an operator applied force P is composed of components due to translation and rotation of the cube

$$F_{S_1} = \frac{P}{4} + \frac{M}{4a} \quad \text{where } M = Pd \quad (19)$$

Making the indicated substitution, Equation (19) may be rewritten in more convenient form as

$$F_{S_1} = \frac{P}{4} \left(1 + \frac{d}{a} \right) > 0 \quad (20)$$

The quantity in parentheses indicates that a compressive force is applied to the sensor, thus it will produce an electrical output. Using the same methodology for the remaining sensors, the following equations apply.

$$F_{S_2} = \frac{P}{4} \left(1 - \frac{d}{a}\right) < 0 \quad (21)$$

$$F_{S_3} = \frac{P}{4} \left(-1 + \frac{d}{a}\right) > 0 \quad (22)$$

$$F_{S_4} = \frac{P}{4} \left(-1 - \frac{d}{a}\right) < 0 \quad (23)$$

For a pure moment M about the Y axis

$$F_{S_2} = F_{S_4} = \frac{M}{4a} \quad (24)$$

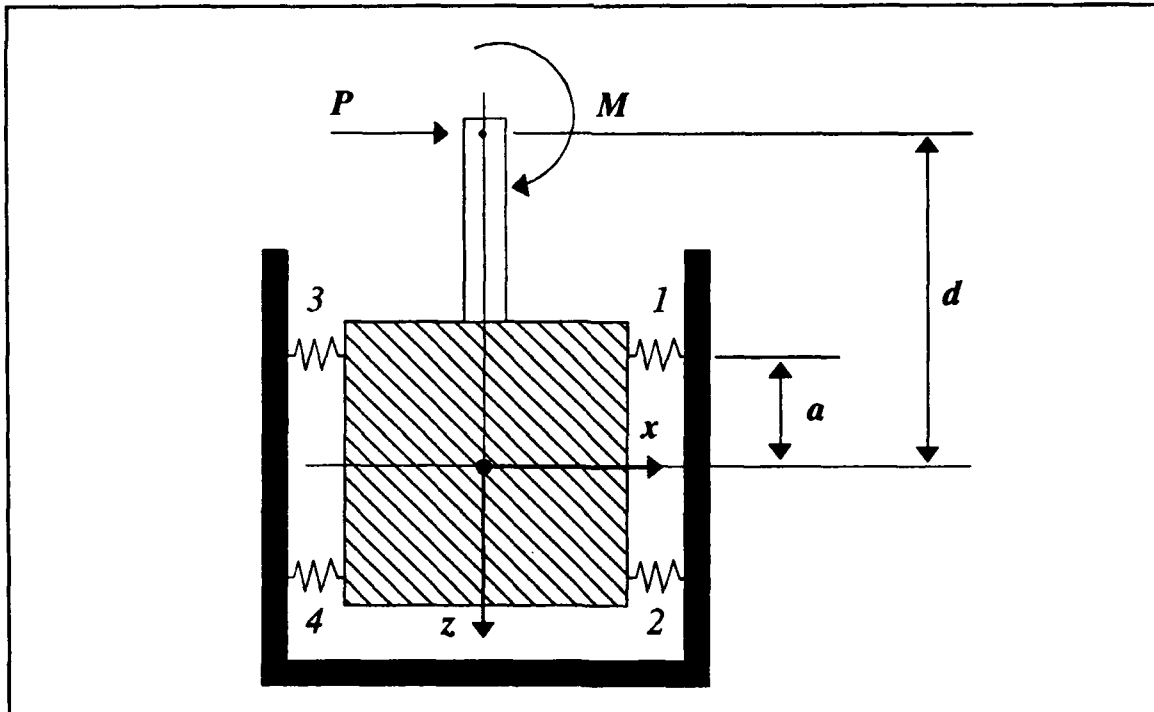


Figure 10. Planar Joystick

Noting from Figure 10 that $d/a > 1$, it is apparent from the above equations that for an applied force P , sensors 1 and 3 are in compression while sensors 2 and 4 are in tension. Because only a compressive force produces an the FSR response, the a_{ij} for sensors 2 and 4 due to P are zero. It is this methodology that is used hereafter to determine the active sensors for a given force or moment and to determine the sensor coefficient matrix A , where a_{ij} are computed by the applicable general formulae

$$a_{ij(P)} = C(\pm \frac{1}{n_t} + \frac{d}{n_r a}) \quad (25)$$

$$a_{ij(M)} = C(\frac{1}{n_r a}) \quad (26)$$

where, considering individual FSR's to be represented by springs, n_t is the number of springs which deflect due to translation of the cube; n_r is the number of springs which deflect due to pure rotation of the cube; and C is some arbitrary scaling constant such that the coefficient matrix is wholly comprised of integers.

5. Sensor Placement

a. Methodology

The first several attempts to solve the problem of sensor placement were approached in an intuitive manner. Building on the planar case of the previous section, four more sensors were added as depicted in Figure 11. Referring to the

planar joystick procedure of the previous section, the same principle of determining the active sensors for a given force/moment applies. The tabular format in Table 2 was used for the various sensor configurations to determine the sensor coefficient matrix. A d/a ratio of 5 was assumed with a equal to 1.

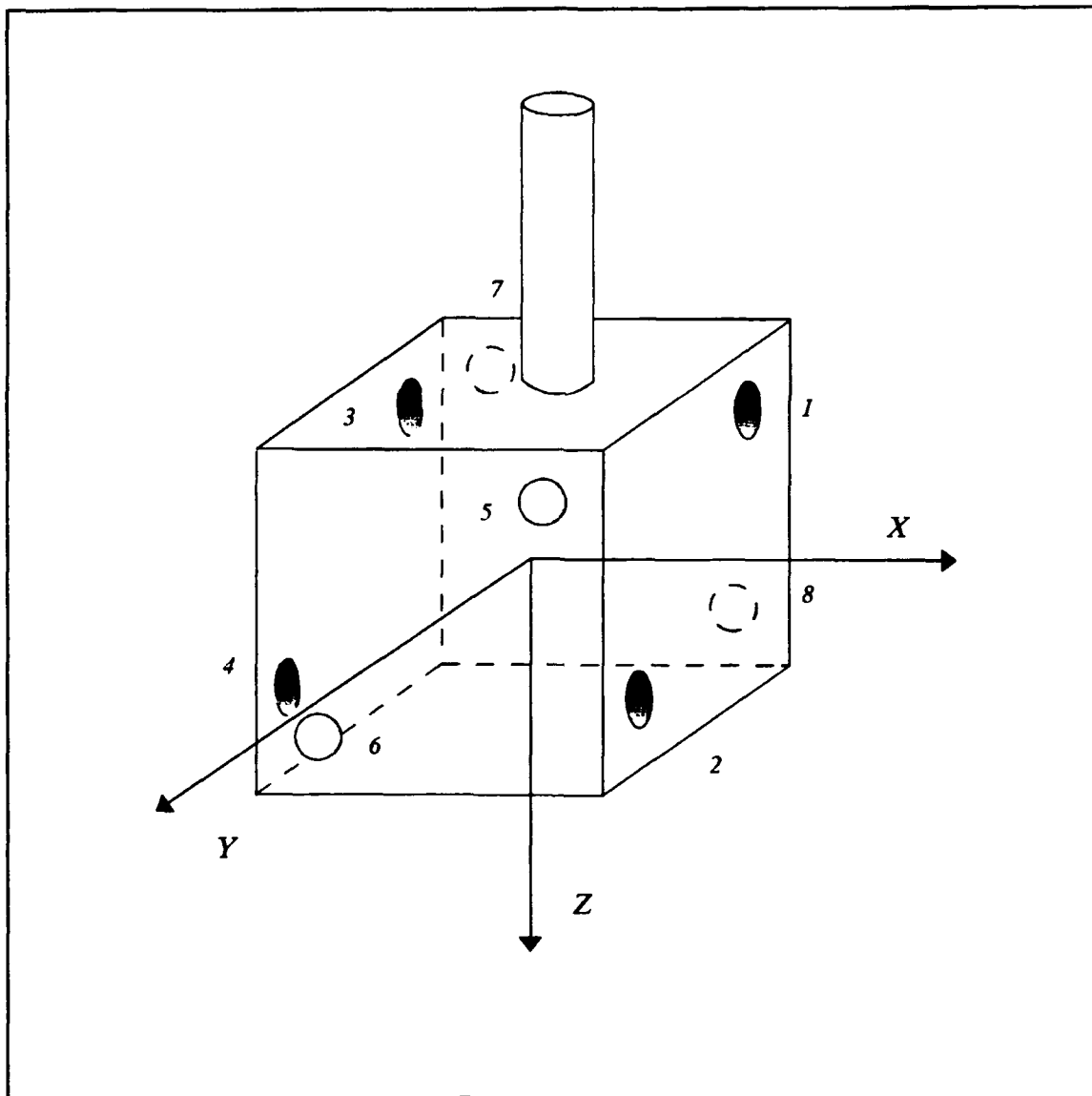


Figure 11. Transducer with 8 Sensors

TABLE 2. BIPLANAR TRANSDUCER COEFFICIENT ARRAY

	S_1	S_2	S_3	S_4	S_5	S_6	S_7	S_8
F_x^+	6/4	0	0	1	0	0	0	0
F_x^-	0	1	6/4	0	0	0	0	0
F_y^+	0	0	0	0	6/4	0	0	1
F_y^-	0	0	0	0	0	1	6/4	0
M_x^+	0	0	0	0	1/4	0	0	1/4
M_x^-	0	0	0	0	0	1/4	1/4	0
M_y^+	0	1/4	1/4	0	0	0	0	0
M_y^-	1/4	0	0	1/4	0	0	0	0

The coefficient matrix A is the transpose of the 8x8 array in Table 2

$$A = \begin{vmatrix} 6 & 0 & 0 & 0 & 0 & 0 & 0 & 1 \\ 0 & 4 & 0 & 0 & 0 & 0 & 1 & 0 \\ 0 & 6 & 0 & 0 & 0 & 0 & 1 & 0 \\ 4 & 0 & 0 & 0 & 0 & 0 & 0 & 1 \\ 0 & 0 & 6 & 0 & 1 & 0 & 0 & 0 \\ 0 & 0 & 0 & 4 & 0 & 1 & 0 & 0 \\ 0 & 0 & 0 & 6 & 0 & 1 & 0 & 0 \\ 0 & 0 & 4 & 0 & 1 & 0 & 0 & 0 \end{vmatrix} \quad (27)$$

where the matrix has been multiplied by a constant (4) for convenience. S is given by the transpose of the first row and F by the first column of Table 2. If A is full rank then F may be calculated by

$$F = A^{-1}S \quad (28)$$

Using the software program *MATLAB*, the rank was calculated to be 8, indicating that all force and moment components may be determined using Equation (28). Attempting to determine additional force or moment components with this sensor configuration is not possible because the minimum number of sensors must be equal to or greater than the number of force/moment components to be determined.

Having mathematically proven the ability to determine eight force and moment components with this sensor configuration, the next step was to add four more sensors, two to both the positive and negative *Z* faces in the same diagonal pattern as illustrated in Figure 12. Taking the transpose of the 12x12 array in Table 3 yields the *A* matrix in Equation (29). From *MATLAB*, the rank of this matrix is 10, indicating that all force and moment components cannot be identified.

Numerous attempts to intuitively solve the rank deficiency problem by repositioning the sensors proved unsuccessful, so a new approach was taken. Nine sensors were placed on each face of the cube for a total of 54 sensors as illustrated in Figure 13. For a force *P* applied to the joystick the sensor output is composed of components due to translation and rotation of the cube. The component due to translation for a single sensor is *P/18*. The component due to

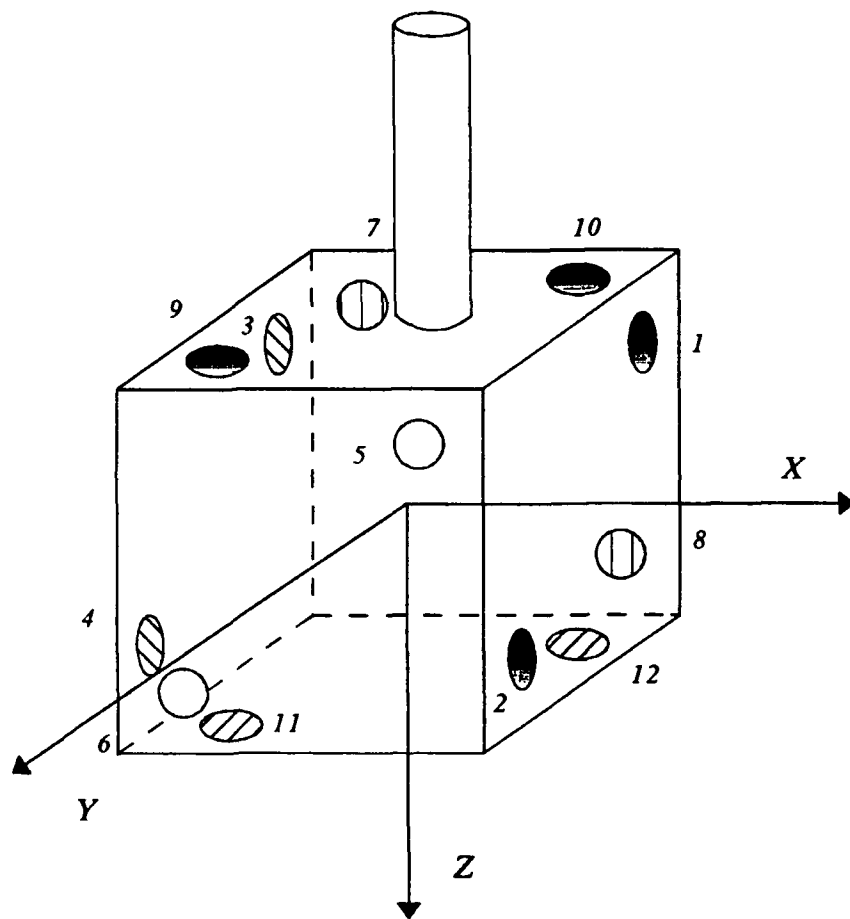


Figure 12. Six Axis Transducer

TABLE 3. SIX AXIS TRANSDUCER COEFFICIENT ARRAY

	S ₁	S ₂	S ₃	S ₄	S ₅	S ₆	S ₇	S ₈	S ₉	S ₁₀	S ₁₁	S ₁₂
F _x ⁺	7	0	0	3	0	0	0	0	0	0	0	0
F _x ⁻	0	3	7	0	0	0	0	0	0	0	0	0
F _y ⁺	0	0	0	0	7	0	0	3	0	0	0	0
F _y ⁻	0	0	0	0	0	3	7	0	0	0	0	0
F _z ⁺	0	0	0	0	0	0	0	0	0	0	2	2
F _z ⁻	0	0	0	0	0	0	0	0	2	2	0	0
M _x ⁺	0	0	0	0	1	0	0	1	0	1	1	0
M _x ⁻	0	0	0	0	0	1	1	0	1	0	0	1
M _y ⁺	0	1	1	0	0	0	0	0	1	0	0	1
M _y ⁻	1	0	0	1	0	0	0	0	0	1	1	0
M _z ⁺	0	1	0	1	0	1	0	1	0	0	0	0
M _z ⁻	1	0	1	0	1	0	1	0	0	0	0	0

$$A = \begin{vmatrix} 7 & 0 & 0 & 0 & 0 & 0 & 0 & 0 & 0 & 1 & 0 & 1 \\ 0 & 3 & 0 & 0 & 0 & 0 & 0 & 0 & 1 & 0 & 1 & 0 \\ 0 & 7 & 0 & 0 & 0 & 0 & 0 & 0 & 1 & 0 & 0 & 1 \\ 3 & 0 & 0 & 0 & 0 & 0 & 0 & 0 & 0 & 1 & 1 & 0 \\ 0 & 0 & 7 & 0 & 0 & 0 & 1 & 0 & 0 & 0 & 0 & 1 \\ 0 & 0 & 0 & 3 & 0 & 0 & 0 & 1 & 0 & 0 & 1 & 0 \\ 0 & 0 & 0 & 7 & 0 & 0 & 0 & 1 & 0 & 0 & 0 & 1 \\ 0 & 0 & 3 & 0 & 0 & 0 & 1 & 0 & 0 & 0 & 1 & 0 \\ 0 & 0 & 0 & 0 & 0 & 2 & 0 & 1 & 1 & 0 & 0 & 0 \\ 0 & 0 & 0 & 0 & 0 & 2 & 1 & 0 & 0 & 1 & 0 & 0 \\ 0 & 0 & 0 & 0 & 2 & 0 & 1 & 0 & 0 & 1 & 0 & 0 \\ 0 & 0 & 0 & 0 & 2 & 0 & 0 & 1 & 1 & 0 & 0 & 0 \end{vmatrix} \quad (29)$$

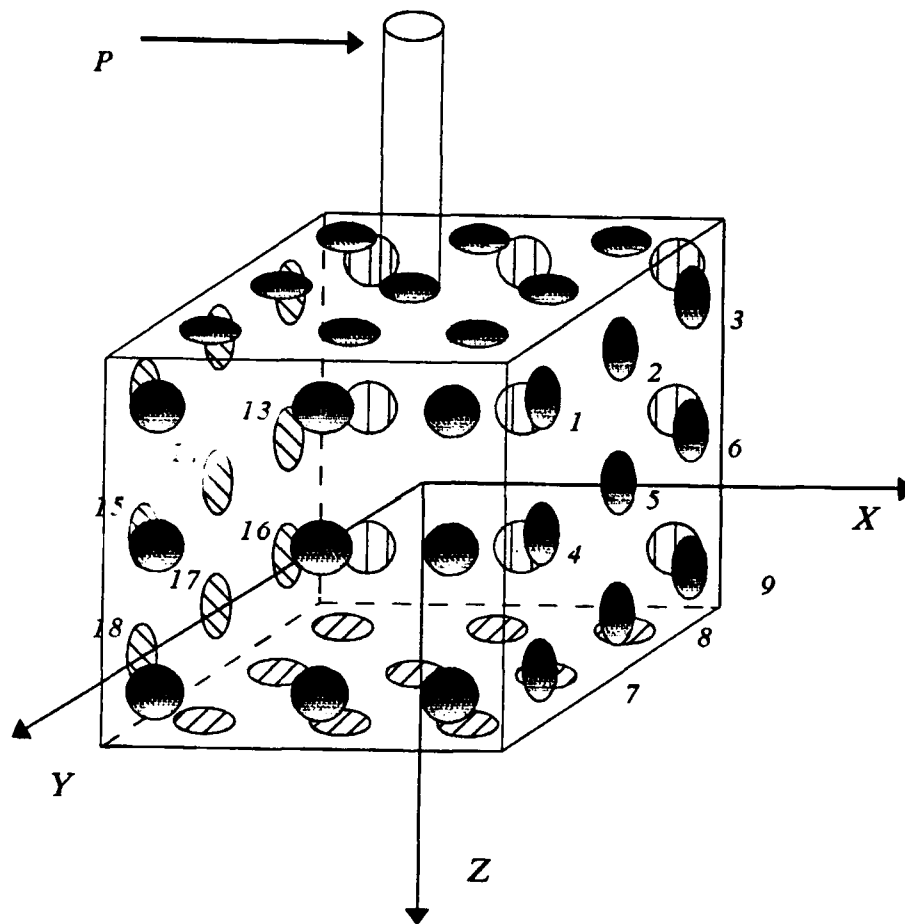


Figure 13. 54 Sensor Transducer

rotation for a single sensor is $M/24a$ where the sensors along the axis of rotation are assumed to see neither a compressive or tensile force. Likewise, the output of a single sensor due to a pure moment or torque (M) is $M/24a$. This results in a slight modification of the basic planar joystick sensor equations. For the illustrated example of a force applied in the positive X direction

$$F_{S_{1,2,3}} = \frac{P}{18} + \frac{M}{24a} \quad (30)$$

$$F_{S_{16,17,18}} = -\frac{P}{18} + \frac{M}{24a} \quad (31)$$

$$F_{S_{4,5,6}} = \frac{P}{18} \quad (32)$$

which if multiplied by a convenient constant (72) become

$$F_{S_{1,2,3}} = P(4 + \frac{3d}{a}) \quad (33)$$

$$F_{S_{16,17,18}} = P(-4 + \frac{3d}{a}) \quad (34)$$

$$F_{S_{4,5,6}} = P(4) \quad (35)$$

For a pure moment about the $-Y$ axis

$$F_{S_{1,2,3}} = F_{S_{16,17,18}} = \frac{M}{24a} \quad (36)$$

which when multiplied by the same constant becomes

$$F_{S_{1,2,3}} = F_{S_{16,17,18}} = \frac{3M}{a} \quad (37)$$

Utilizing Equations (33) through (35) and (37) yields the 54x12 **A** matrix given in Appendix A. Premultiplying this matrix by its transpose and using *MATLAB* to compute the rank of **A^TA** resulted in a full rank coefficient matrix (12).

b. Transducer Design Optimization

Having proven the solvability of this problem using 54 sensors and knowing the minimum number of sensors to be 12, the next logical step was to attempt to optimize the design by eliminating unnecessary sensors, if any. Rather than eliminating sensors one at a time, a selective elimination pattern was used to eliminate groups of sensors from each face. The steps of this trial and error process are detailed in Appendix A. This elimination process was performed without making any modifications to the basic sensor equations. The end result was achievement of the global minimum for the number of sensors. It should be noted that the resulting placement pattern is not a unique solution, but rather a particular solution. A different sensor elimination strategy may well result in a different placement pattern. The placement of sensors is depicted in Figure 14 and the unmodified coefficient matrix given by Equation (38). As a check, a modified **A** matrix which is based on 12 rather than 54 sensors was computed (Equation 39) with the rank remaining 12.

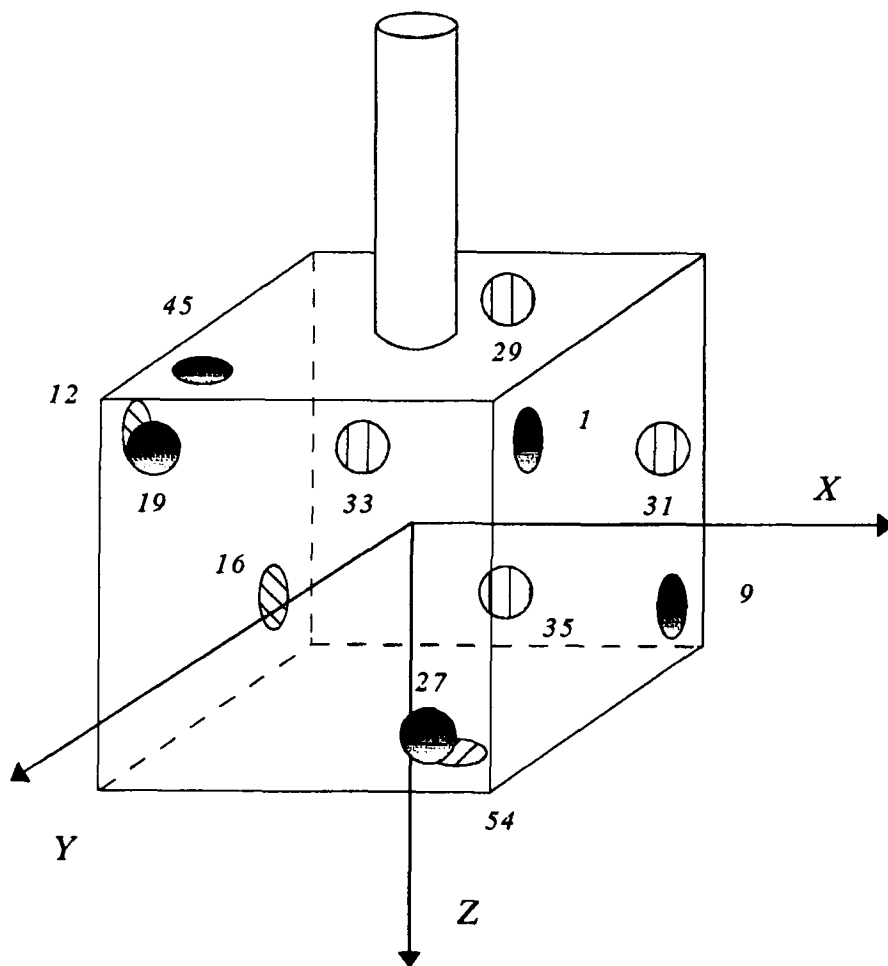


Figure 14. Optimized Full Order Transducer

$$A = \begin{vmatrix} 19 & 0 & 0 & 0 & 0 & 0 & 0 & 0 & 0 & 3 & 0 & 3 \\ 0 & 11 & 0 & 0 & 0 & 0 & 0 & 0 & 3 & 0 & 3 & 0 \\ 0 & 19 & 0 & 0 & 0 & 0 & 0 & 0 & 3 & 0 & 3 & 0 \\ 11 & 0 & 0 & 0 & 0 & 0 & 0 & 0 & 0 & 3 & 0 & 3 \\ 0 & 0 & 19 & 0 & 0 & 0 & 3 & 0 & 0 & 0 & 0 & 3 \\ 0 & 0 & 0 & 11 & 0 & 0 & 0 & 3 & 0 & 0 & 3 & 0 \\ 0 & 0 & 0 & 19 & 0 & 0 & 0 & 3 & 0 & 0 & 0 & 0 \\ 0 & 0 & 0 & 4 & 0 & 0 & 0 & 0 & 0 & 0 & 0 & 3 \\ 0 & 0 & 0 & 4 & 0 & 0 & 0 & 0 & 0 & 0 & 3 & 0 \\ 0 & 0 & 11 & 0 & 0 & 0 & 3 & 0 & 0 & 0 & 0 & 0 \\ 15 & 0 & 0 & 15 & 0 & 4 & 0 & 3 & 0 & 3 & 0 & 0 \\ 15 & 0 & 15 & 0 & 4 & 0 & 3 & 0 & 0 & 3 & 0 & 0 \end{vmatrix} \quad (38)$$

$$A = \begin{vmatrix} 26 & 0 & 0 & 0 & 0 & 0 & 0 & 0 & 0 & 4 & 0 & 3 \\ 0 & 14 & 0 & 0 & 0 & 0 & 0 & 0 & 4 & 0 & 3 & 0 \\ 0 & 26 & 0 & 0 & 0 & 0 & 0 & 0 & 4 & 0 & 4 & 0 \\ 14 & 0 & 0 & 0 & 0 & 0 & 0 & 0 & 0 & 4 & 0 & 3 \\ 0 & 0 & 24 & 0 & 0 & 0 & 4 & 0 & 0 & 0 & 0 & 3 \\ 0 & 0 & 0 & 16 & 0 & 0 & 0 & 4 & 0 & 0 & 3 & 0 \\ 0 & 0 & 0 & 24 & 0 & 0 & 0 & 4 & 0 & 0 & 0 & 0 \\ 0 & 0 & 0 & 4 & 0 & 0 & 0 & 0 & 0 & 0 & 0 & 3 \\ 0 & 0 & 0 & 4 & 0 & 0 & 0 & 0 & 0 & 0 & 3 & 0 \\ 0 & 0 & 16 & 0 & 0 & 0 & 4 & 0 & 0 & 0 & 0 & 0 \\ 20 & 0 & 0 & 20 & 0 & 12 & 0 & 4 & 0 & 4 & 0 & 0 \\ 20 & 0 & 20 & 0 & 12 & 0 & 4 & 0 & 0 & 4 & 0 & 0 \end{vmatrix} \quad (39)$$

c. Reduced Order Transducer

Not all manipulator tasks utilizing force control require a full order force-torque transducer. Having calculated one feasible placement strategy, the next step was to determine the optimal placement for a reduced order transducer capable of detecting three forces (in both the positive and negative directions) and a moment (positive and

negative) about the Z axis. Once again sensors were eliminated on a trial and error basis until further elimination of any sensors resulted in a rank deficient coefficient matrix. From the derived sensor pattern a reduced order prototype was designed with the sensor placement pattern depicted in Figure 15. The following equation applies to the reduced order transducer. Equation (41) gives the modified A matrix.

$$\begin{bmatrix} S_1 \\ S_2 \\ S_3 \\ S_4 \\ S_5 \\ S_6 \\ S_7 \\ S_8 \end{bmatrix} = \begin{bmatrix} 19 & 0 & 0 & 0 & 0 & 0 & 0 & 3 \\ 0 & 19 & 0 & 0 & 0 & 0 & 0 & 3 \\ 0 & 0 & 19 & 0 & 0 & 0 & 0 & 3 \\ 0 & 0 & 0 & 19 & 0 & 0 & 0 & 0 \\ 0 & 0 & 0 & 4 & 0 & 0 & 0 & 3 \\ 0 & 0 & 0 & 4 & 0 & 0 & 3 & 0 \\ 0 & 15 & 15 & 0 & 0 & 4 & 0 & 0 \\ 0 & 15 & 0 & 15 & 4 & 0 & 0 & 0 \end{bmatrix} \begin{bmatrix} F_x^+ \\ F_x^- \\ F_y^+ \\ F_y^- \\ F_z^+ \\ F_z^- \\ M_z^+ \\ M_z^- \end{bmatrix} \quad (40)$$

$$A = \begin{bmatrix} 35 & 0 & 0 & 0 & 0 & 0 & 0 & 4 \\ 0 & 35 & 0 & 0 & 0 & 0 & 0 & 4 \\ 0 & 0 & 30 & 0 & 0 & 0 & 0 & 4 \\ 0 & 0 & 0 & 30 & 0 & 0 & 0 & 0 \\ 0 & 0 & 0 & 5 & 0 & 0 & 0 & 4 \\ 0 & 0 & 0 & 5 & 0 & 0 & 4 & 0 \\ 0 & 5 & 5 & 0 & 0 & 10 & 0 & 0 \\ 0 & 5 & 0 & 5 & 10 & 0 & 0 & 0 \end{bmatrix} \quad (41)$$

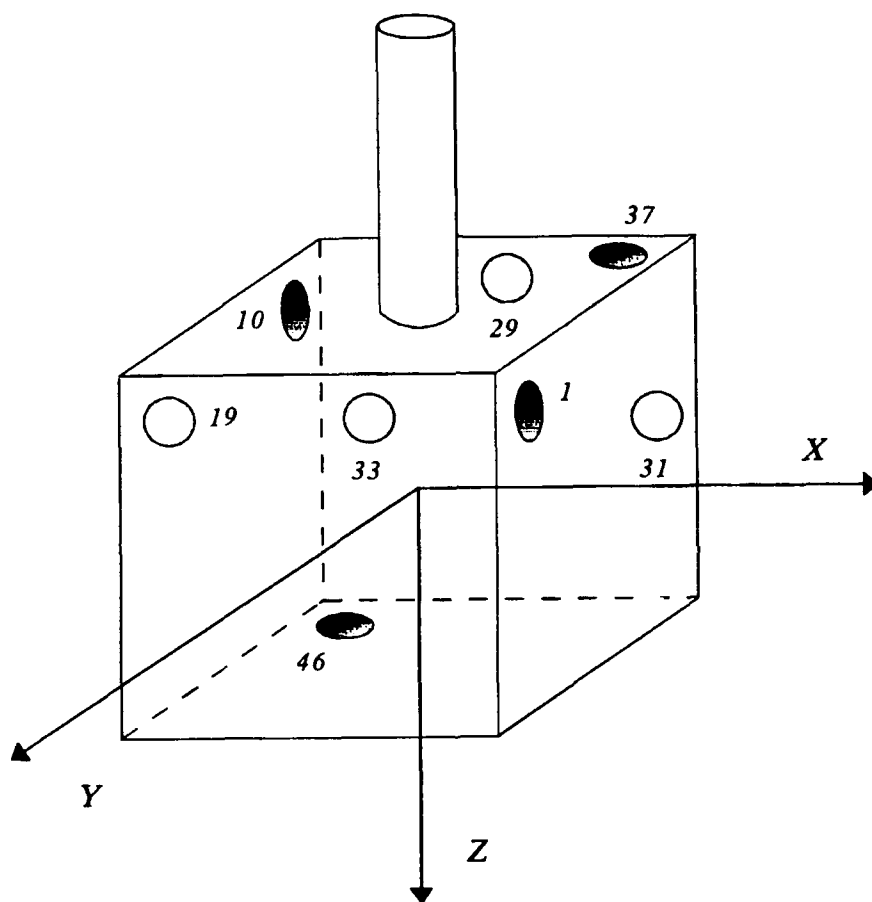


Figure 15. Reduced Order Transducer

B. PROTOTYPE TRANSDUCER DESIGN

1. Mechanical Design

Some manipulator tasking problems requiring force control do not require the use of a full order force-torque transducer. If for example, the manipulator is used to apply a specific torque to a screw, the primary consideration is the ability to measure the torque about the z axis of the transducer coordinate frame. Using the sensor placement pattern developed in the previous section for the reduced order transducer simplifies the electronic interface problem and successful implementation using the *PUMA 560* will verify the theory developed in the previous section.

Because of the weight limitations of the *PUMA*, the mechanical design of the prototype sensor had to be carefully considered. For simplicity, aluminum stock materials were used. The choice of aluminum minimized weight while satisfying the requirement that the *FSR's* be mounted on a firm backing. The only other constraints were the size of the *FSR's* and the wiring requirements. An isometric drawing of the mechanical design is depicted in Figure 16a. Engineering specifics are provided in a plan view diagram of the prototype given in Figure 16b.

Mounting of the sensors on the aluminum cube proved to be somewhat of a problem initially. After cleaning the surface of the cube with acetone followed by alcohol, *M-Bond 200* was

used to secure the sensors. Upon completion, the sensors were tested for response and found to be inoperable. The epoxy was apparently incompatible with the substrate of the FSR. New sensors were then mounted using a microthin double sided adhesive produced by 3-M. After verifying proper response characteristics, the individual sensors were then wired using 16 wire ribbon cable and then electrically insulated using an air curing 3140 sealant. Table 4 provides the wiring code for individual sensors.

TABLE 4. PROTOTYPE TRANSDUCER WIRING CODE

<i>Sensor Location</i>	<i>Sensor Number</i>	<i>Mounting Face</i>	<i>Wiring Color Code</i>
1	1	+X	orange/orange
19	2	+Y	yellow/yellow
10	3	-X	green/green
29	4	-Y	blue/blue
31	5	-Y	white/black
33	6	-Y	brown/brown
37	7	-Z	red/red
46	8	+Z	gray/purple

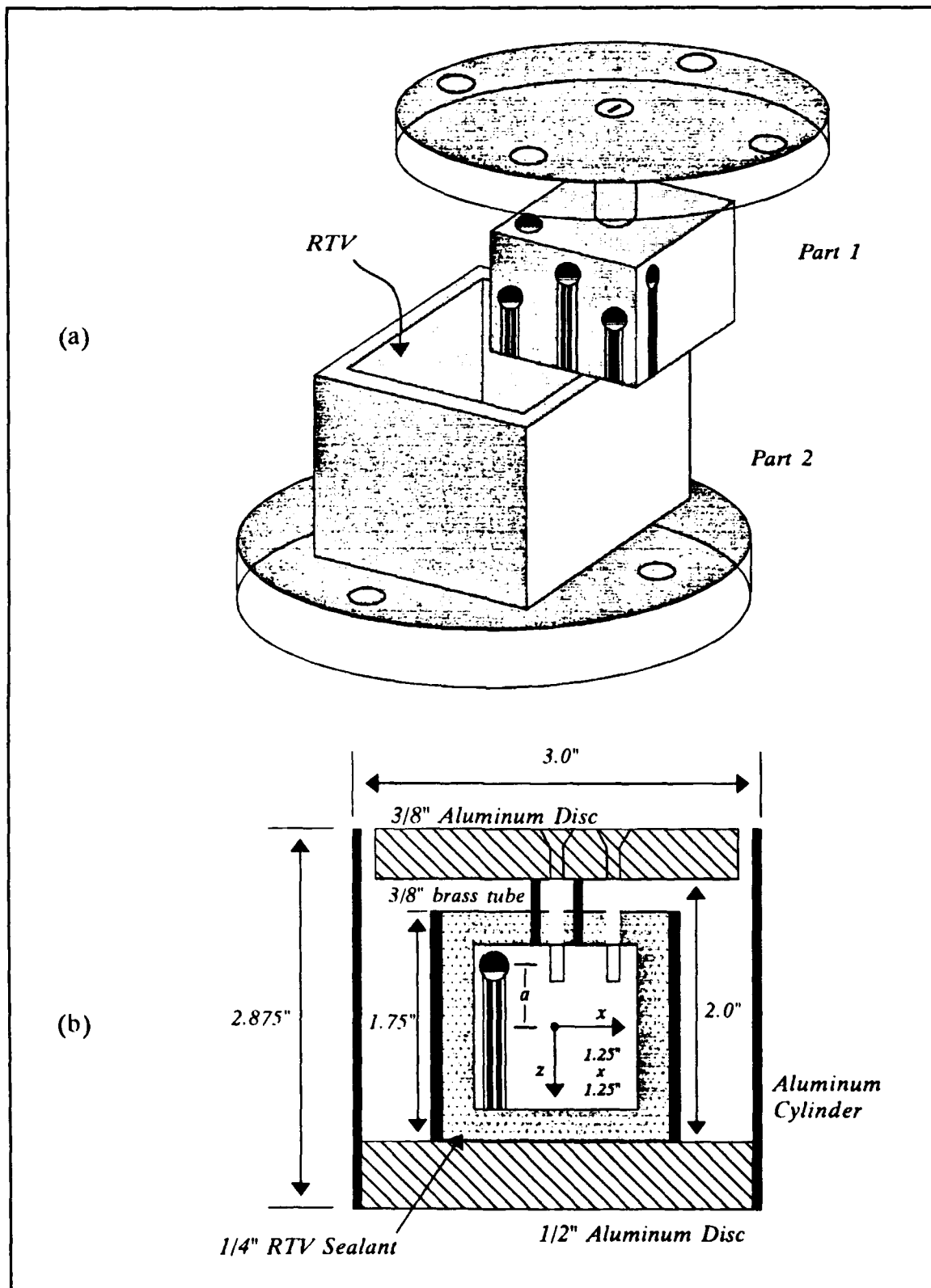


Figure 16. Prototype Transducer Mechanical Design

2. Transducer Testing and Calibration

Sensor leads were wired to an analog to digital data translation board in a voltage divider configuration with a 20 volt range (-10v to +10v) to increase sensitivity. The data board was then connected to a Zenith 286PC for data acquisition using the program GRABDAT. However, despite satisfactory sensor response tests after the mounting and wiring procedures and again after sealing the sensors electrically with an RTV sealant, when the transducer was setup for calibration two sensors failed to provide any response. Two more provided only intermittent response indicating the presence of shorts. Referring to Table 4 and Figure 15, the four remaining sensors with good response characteristics were sensors 1, 4, 5 and 6. Though not capable of detecting the six force and two moment components it was designed to detect, the transducer is capable of detecting two force and two moment components as shown in Table 5.

TABLE 5. OPERABLE SENSOR COEFFICIENT ARRAY

	S_1	S_4	S_5	S_6
F_x^+	$(1 + d/a)$	0	0	0
F_y^-	0	$(1/3 + d/a)$	1/3	1/3
M_z^+	0	0	0	1/3a
M_z^-	1/3a	0	1/3a	0

where a is 15/32", d is 1.5" plus the length of the arm, and the coefficient matrix A is the transpose of the 4x4 array.

Calibration of the transducer prototype for these components is warranted as it will adequately validate the concept for a 7 order transducer. This procedure may be accomplished by placing the transducer in an indexing chuck and applying a known weight in each direction of the six axis transducer coordinate frame.

IV. FORCE CONTROL

A. THEORY

1. Robotic Application of Transducer

The transducer discussed in the previous chapter may be utilized with a robotic manipulator arm such as the *PUMA 560 6R Manipulator* in two different ways as depicted in Figure 17. First, it may be used as a joystick in force override control mode to reflect desired forces or torques in the tool frame. Secondly, it may be attached in the wrist frame to sense the actual force or torque being applied and fed back to the controller to produce a force error signal. The following sections provide the development for general manipulator mechanics and a method by which a force error signal may be utilized to achieve force reflection in the end-effector.

2. Manipulator Kinematics

a. Generalized Coordinate Transformations

Given a coordinate reference coordinate system $\{A\}$ with three mutually orthogonal unit vectors, any point in space may be located by a position vector [Ref. 5]

$$P^A = p_x i + p_y j + p_z k \quad (42)$$

When dealing with a rigid body such as an end-effector tool it is necessary to know its position and orientation, hereafter referred to as its *pose*, with respect

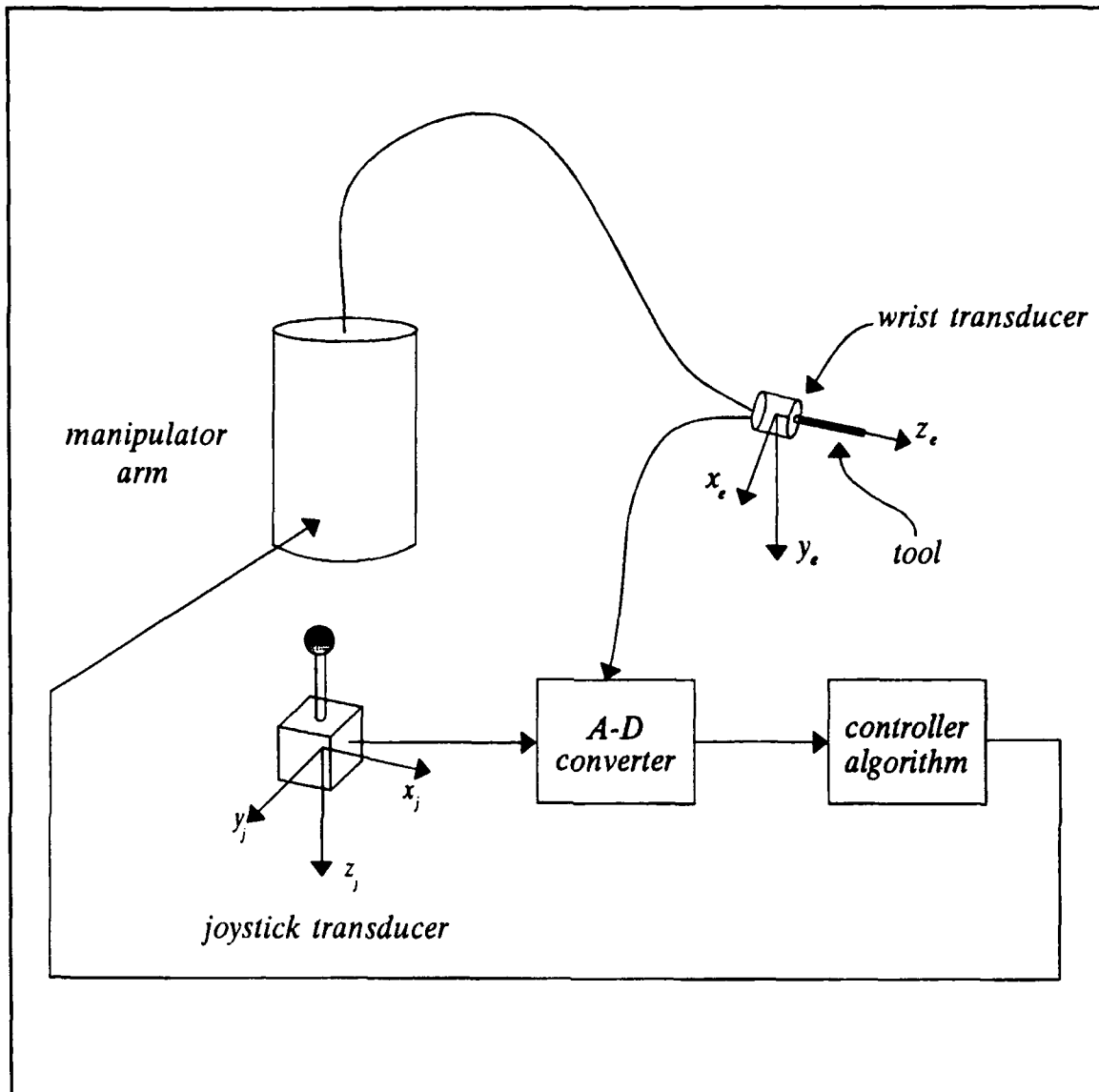


Figure 17. Robotic Application of Transducer

to the reference coordinate system. To determine the orientation it is necessary to attach a coordinate system to the body at some convenient location, for example, a joint or the center of mass. The orientation of the unit vectors of the body-attached coordinate system with respect to the reference system is obtained by taking the vector dot product

of the unit vectors. Writing the unit vectors of coordinate system $\{B\}$ in terms of the reference system produces a 3x3 matrix known as the **rotation matrix**. Because this particular matrix is *orthonormal*, it is useful to note that the inverse of the rotation matrix is equal to its transpose [Ref. 6].

A **frame** is a set of four vectors that represents the pose of a body with respect to some reference system. Mathematically, a frame is a rotation matrix and a position vector which describe one coordinate system relative to another [Ref. 7]. A vector whose description is known in frame $\{B\}$ may be described in frame $\{A\}$ through a process of translational and rotational mapping. Mathematically, description of the vector in the $\{A\}$ frame is accomplished by a transformation matrix operating on P^B , given in compact notation as

$$P^A = T_A^B P^B \quad (43)$$

or in matrix form as

$$\begin{vmatrix} P^A \\ \text{---} \\ 1 \end{vmatrix} = \begin{vmatrix} R_A^B & P_{BORG}^A \\ \text{---} & \text{---} \\ 0 & 0 & 0 & 1 \end{vmatrix} \begin{vmatrix} P^B \\ \text{---} \\ 1 \end{vmatrix} \quad (44)$$

b. Compound Transformations

For a robotic manipulator arm with multiple frame assignments, it is necessary to perform compound coordinate frame transformations [Ref. 8] in order to relate the pose of

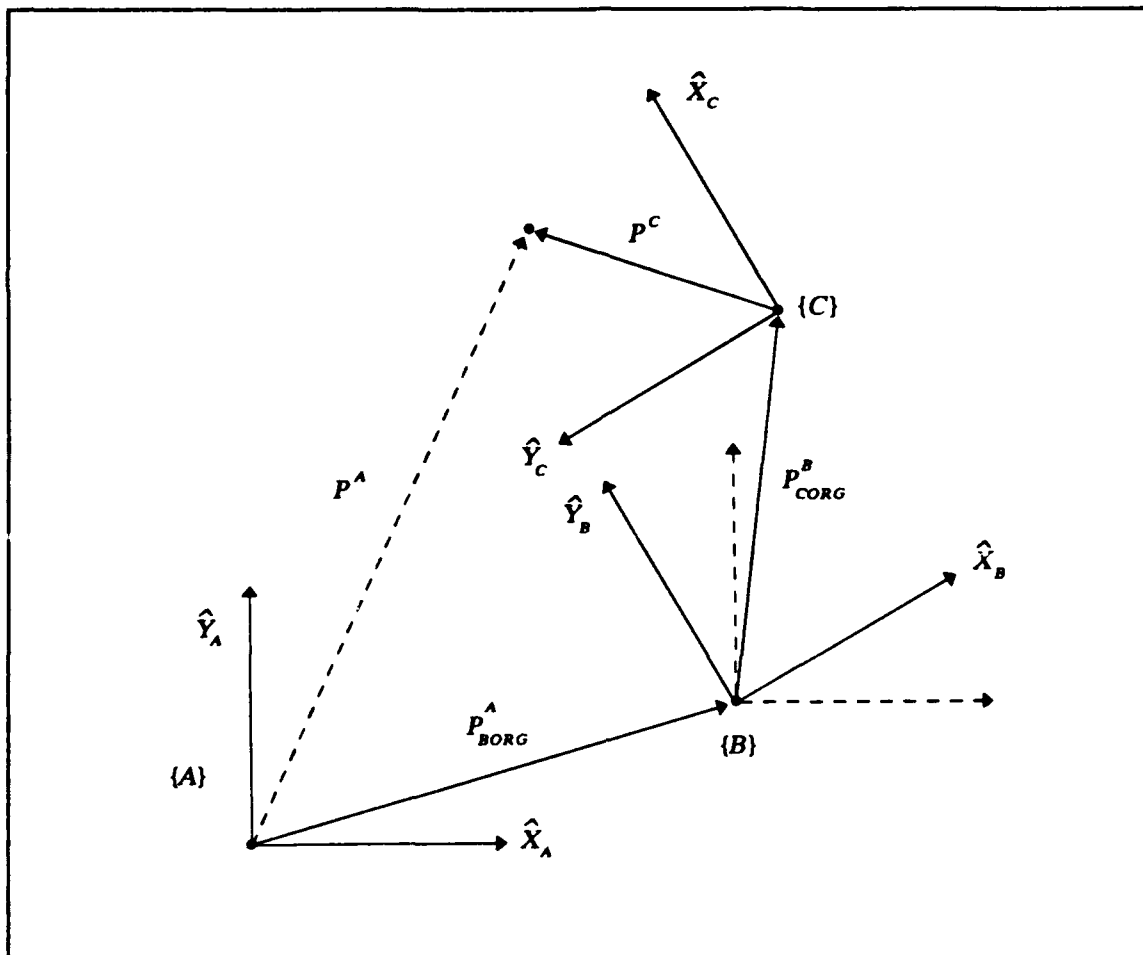


Figure 18. Translated and Rotated Link Frame

the end-effector to the base frame. A generalized example of this process is depicted in Figure 18. With the description of frame $\{C\}$ known relative to frame $\{B\}$, vector P^C can be transformed into $\{B\}$ by

$$P^B = T_C^B P^C \quad (45)$$

which may then be transformed into $\{A\}$ by

$$P^A = T_B^A P^B \quad (46)$$

Combining Equations (45) and (46) yields the following result:

$$P^A = T_B^A T_C^B P^C \quad (47)$$

Generally stated, a vector in any frame may be described in the reference frame by multiplying the vector by the product of individual transformation matrices.

c. Denavit-Hartenberg Transformations

A manipulator arm consists of a series of links connected by revolute or prismatic joints with each link-joint pair constituting 1 degree of freedom. To describe the relative pose of each link in a kinematic chain, Denavit and Hartenberg [1955] proposed a systematic, matrix method approach to the establishment of link coordinate frames. The ***Denavit-Hartenberg*** (*D-H*) method is a convenient and popular convention that results in a *4x4 homogeneous transformation matrix* representing each link's coordinate system at the joint with respect to the previous link's coordinate system. Thus, the end-effector frame for any *n* degree of freedom manipulator may be expressed in reference frame coordinates through a series of sequential transformations. [Ref. 9]

Links are numbered outwardly from the base of the manipulator arm starting with link 0, which is attached to the base frame and not considered part of the system from a kinematic standpoint. Link *n* is the point at which a tool is attached. Thus, an *n* degree of freedom manipulator has *n+1* coordinate frame assignments. The initial frame {0} is

assigned to a convenient location on link 0, often referred to as the base frame $\{B\}$, and serves as an inertial reference frame for the manipulator arm.

Referring to Figure 19, the following general rules apply to the assignment of individual link coordinate frames

1. The z_{i-1} axis lies along the axis of motion of the i^{th} joint.
2. The x_i axis is normal to the z_{i-1} axis, and pointing away from it.
3. The y_i axis completes the right-handed coordinate system as required.

Associated with each link in the kinematic chain of a manipulator for $i = 1, 2, \dots, n$, are two sets of parameters; the joint parameters (d_i and θ_i) which describe the relative positions of neighboring links and the link parameters (a_i and α_i) which physically describe the link. To obtain these parameters a joint axis is established for joint i as depicted in Figure 18. Because the joint connects two links, the joint axis has two normals. The relative position of link i and link $i-1$ along the common joint axis is known as the **link offset** and denoted by d_i . This offset is a variable for a prismatic joint. The **joint angle** θ_i is the degree of rotation about the common axis between neighboring links. For a revolute joint,

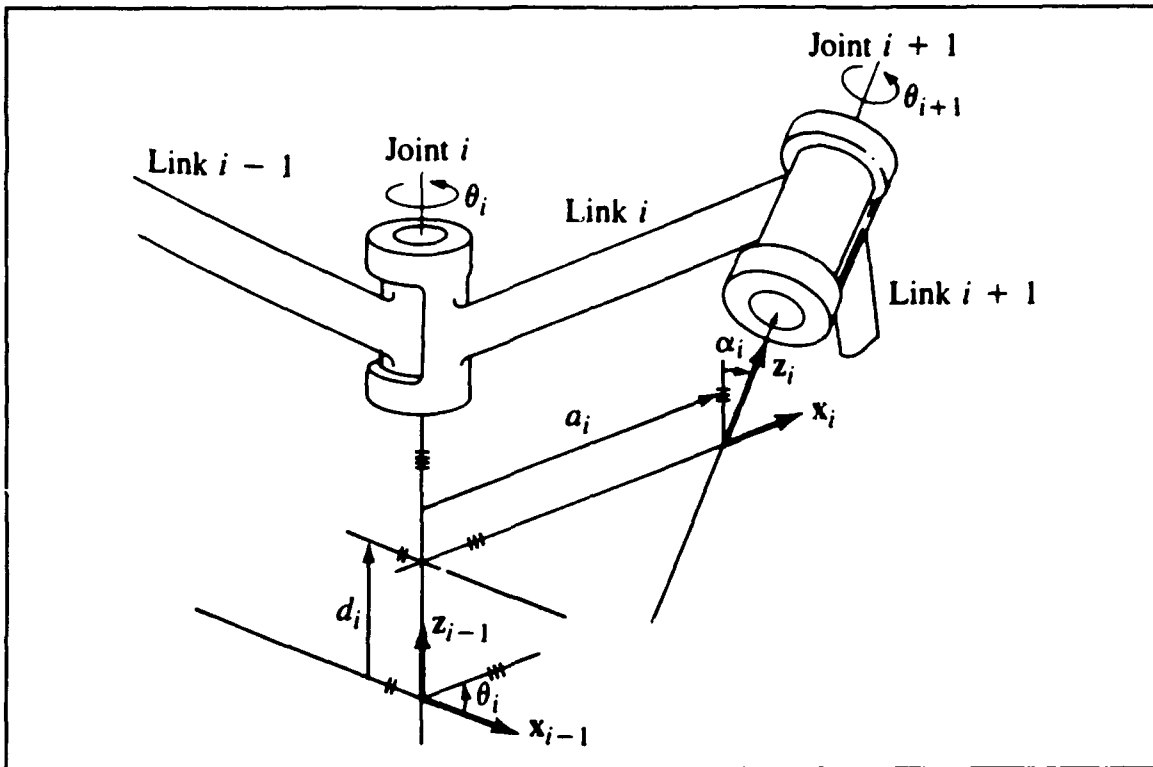


Figure 19. Generic Manipulator Link [Ref. 10]

this parameter is a variable. The **link length** a_i is the distance along the common normal between joint axes. The **link twist** α_i is the angle between the joint axes measured in a plane perpendicular to a_i . Referring to Figure 18, the convention for measuring these parameters is as follows. [Ref. 11]

d_i is the distance from the origin of the $(i-1)^{th}$ coordinate frame to the intersection of the z_{i-1} axis with the x_i axis along the z_{i-1} axis.

θ_i is the joint angle from the x_{i-1} axis to the x_i axis about the z_{i-1} axis (using the right-hand rule).

a_i is the offset distance from the intersection of the z_{i-1} axis with the x_i axis to the origin of the i^{th} frame along the x_i axis.

α_i is the offset angle from the z_{i-1} axis to the z_i axis about the x_i axis (using the right-hand rule).

Again, referring to the diagram for a general link provided in Figure 18, it may be shown that a point in the i^{th} frame may be expressed in the $(i-1)^{th}$ frame by performing a series of four transformations, symbolically represented in Equation (48). The product of these transformations is a composite homogeneous transformation matrix for adjacent link coordinate frames and is known as the **D-H transformation matrix**, given by Equation (47). [Ref. 13]

$$T_i^{i-1} = T_z, d T_z, \theta T_x, a T_x, \alpha \quad (48)$$

$$T_i^{i-1} = \begin{vmatrix} \cos\theta_i & -\cos\alpha_i \sin\theta_i & \sin\alpha_i \sin\theta_i & a_i \cos\theta_i \\ \sin\theta_i & \cos\alpha_i \cos\theta_i & -\sin\alpha_i \cos\theta_i & a_i \sin\theta_i \\ 0 & \sin\alpha_i & \cos\alpha_i & d_i \\ 0 & 0 & 0 & 1 \end{vmatrix} \quad (49)$$

d. PUMA 560 Denavit-Hartenberg Parameters

Within the bounds of the rules for link frame allocation previously stated, different authors have slightly

different conventions for the assignment of these frames. The method applied by Fu [Ref. 12] is adopted here. Link frame assignments for the PUMA 560 are given in Figure 20.

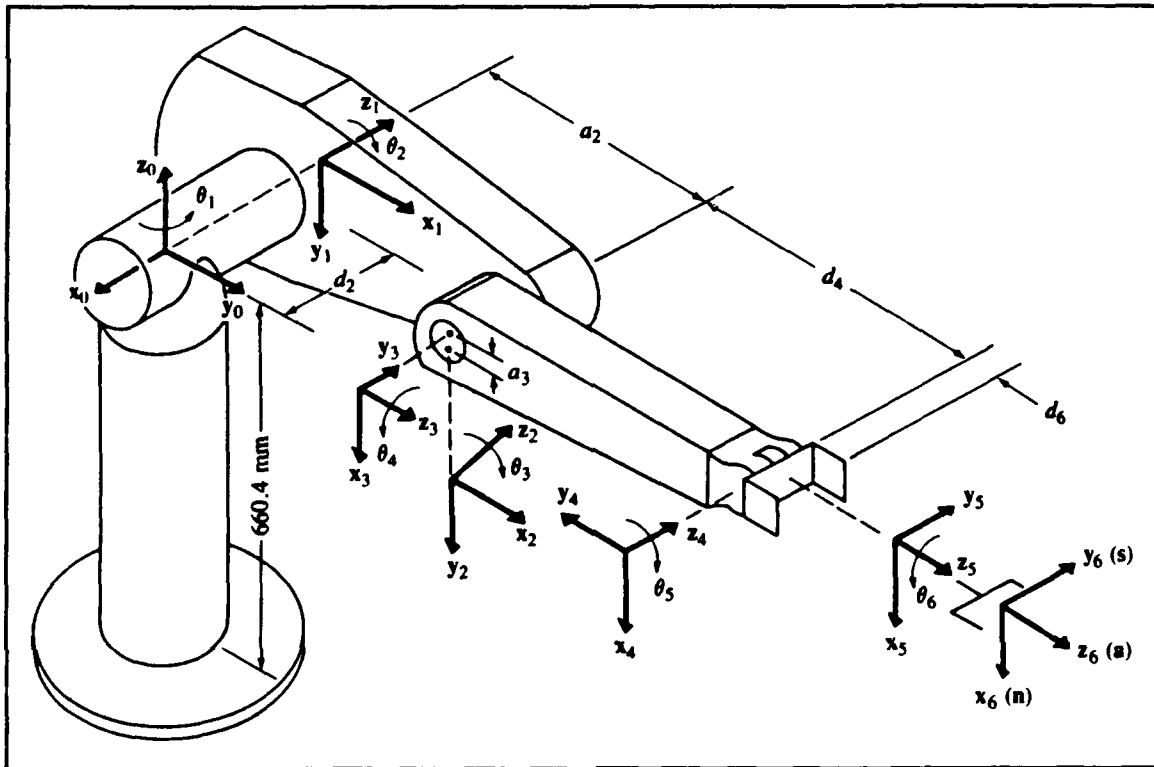


Figure 20. PUMA Link Frame Assignments

TABLE 6. PUMA 560 LINK AND JOINT PARAMETERS

Joint i	θ_i	α_i	a_i (mm)	d_i (mm)
1	90	-90	0	0
2	0	0	431.8	149.09
3	90	90	-20.32	0
4	0	-90	0	433.07
5	0	90	0	0
6	0	0	0	56.25

e. PUMA 560 Forward Kinematics

Kinematics in general is the study of motion without regard for the forces or torques required to produce that motion. The manipulator forward kinematic problem involves the concatenation of neighboring link transforms to solve for the pose of a specific link with respect to the base frame and thus, describes how the relative pose of assigned link coordinate frames change with respect to an inertial reference frame as the manipulator articulates through space.

In the case of the PUMA 560, the pose of frame {6} with respect to {0} may be found by multiplying the following kinematic chain of transformation matrices

$$T_6^0 = T_1^0 T_2^1 T_3^2 T_4^3 T_5^4 T_6^5 \quad (50)$$

Successive multiplication of 4x4 matrices can become quite cumbersome algebraically. In order to simplify this task, it is convenient to multiply the first and second three transformation matrices to form two separate matrices such that

$$T_6^0 = T_3^0 T_6^3 = \begin{bmatrix} r_{11} & r_{12} & r_{13} & p_x \\ r_{21} & r_{22} & r_{23} & p_y \\ r_{31} & r_{32} & r_{33} & p_z \\ 0 & 0 & 0 & 1 \end{bmatrix} \quad (51)$$

in which the 3×1 submatrix $(p_x \ p_y \ p_z)^T$ represents the position of the end-effector and the 3×3 rotation submatrix represents the orientation. The 12 equations that result form the upper three rows of the matrix constitute the forward kinematics of the PUMA 560 manipulator. Individual transformation matrices and the kinematic equations are provided in Appendix B.

f. Inverse Manipulator Kinematics

Whereas the forward kinematic problem is solely concerned with computing the pose of the end-effector with respect to an inertial reference or base frame, the inverse kinematic problem is concerned with computation of the required set of joint angles to produce the desired pose of the end-effector. Recall that the pose of the PUMA end-effector with respect to the base frame is given by the **manipulator transformation matrix**.

$$T_6^0 = \begin{bmatrix} I_{11} & I_{12} & I_{13} & P_x \\ I_{21} & I_{22} & I_{23} & P_y \\ I_{31} & I_{32} & I_{33} & P_z \\ 0 & 0 & 0 & 1 \end{bmatrix} = T_1^0(\theta_1) T_2^1(\theta_2) T_3^2(\theta_3) T_4^3(\theta_4) T_5^4(\theta_5) T_6^5(\theta_6) \quad (52)$$

The resulting kinematic equations are nonlinear, transcendental equations that at best are difficult to solve. From Equation (52) there are twelve equations and six unknown joint angles, indicating the possibility of multiple solutions [Ref. 14]. The **inverse transform technique** for obtaining the

joint angles involves sequential inversion of the individual transformation matrices and equating matrix elements to obtain a trigonometric relationship for the individual joint angle (numerical methods may also be employed). For example, to solve for θ_1

$$[T_1^0(\theta_1)]^{-1} T_6^0 = T_2^1(\theta_2) T_3^2(\theta_3) T_4^3(\theta_4) T_5^4(\theta_5) T_6^5(\theta_6) \quad (53)$$

where the indicated transformation matrix inverse can be found from

$$[T_i^{i-1}]^{-1} = T_{i-1}^i = \begin{vmatrix} \cos\theta_i & \sin\theta_i & 0 & -a_i \\ -\cos\alpha_i \sin\theta_i & \cos\alpha_i \cos\theta_i & \sin\alpha_i & -d_i \sin\alpha_i \\ \sin\alpha_i \sin\theta_i & -\sin\alpha_i \cos\theta_i & \cos\alpha_i & -d_i \cos\alpha_i \\ 0 & 0 & 0 & 1 \end{vmatrix} \quad (54)$$

rewriting Equation (53)

$$\begin{vmatrix} \cos\theta_1 & \sin\theta_1 & 0 & 0 \\ 0 & 0 & -1 & 0 \\ -\sin\theta_1 & \cos\theta_1 & 0 & 0 \\ 0 & 0 & 0 & 1 \end{vmatrix} \begin{vmatrix} r_{11} & r_{12} & r_{13} & p_x \\ r_{21} & r_{22} & r_{23} & p_y \\ r_{31} & r_{32} & r_{33} & p_z \\ 0 & 0 & 0 & 1 \end{vmatrix} = T_6^1 \quad (55)$$

Performing the indicated matrix multiplication and following the methodology outlined by Craig [Ref. 15] of equating elements from both sides of Equation (55) and making use of several trigonometric substitutions and identities, a solution

may be obtained for θ_1 . Joint angles θ_2 through θ_6 are obtained in a similar manner.

3. Jacobian Development

a. Static Forces in Manipulators

As with any other static structure the forces and moments in each link must balance at any given instant. To determine the static forces in the manipulator it is necessary to write force and moment equations for each individual link. From these equations the required joint torque for each link to maintain static equilibrium may be computed. [Ref. 16] Figure 20 depicts the free body diagram for a generic link

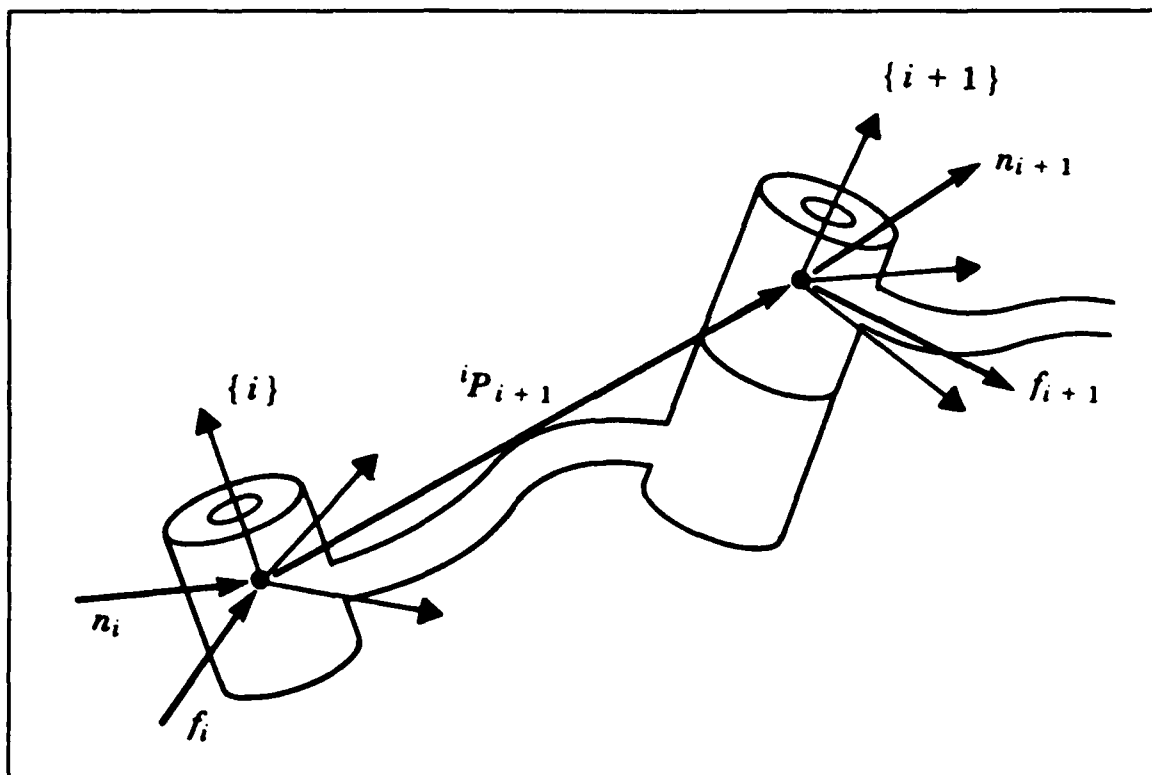


Figure 21. Forces on a Manipulator Link

where \mathbf{f}_i and \mathbf{n}_i are force and torque respectively exerted on link i by link $i-1$. Summing forces and moments and setting equal to zero yields the following results:

$$\mathbf{f}_i^i = \mathbf{f}_{i+1}^i \quad (56)$$

$$\mathbf{n}_i^i = \mathbf{n}_{i+1}^i + \mathbf{P}_{i+1}^i \times \mathbf{f}_{i+1}^i \quad (57)$$

These equations may be written in terms of only forces and moments within their own link coordinate frames by multiplying the right side of each equation by the rotation matrix that describes link frame $\{i+1\}$ relative to $\{i\}$. These equations are applied starting from the last link of the manipulator and proceeding inward.

$$\mathbf{f}_i^i = \mathbf{R}_{i+1}^i \mathbf{f}_{i+1}^{i+1} \quad (58)$$

$$\mathbf{n}_i^i = \mathbf{R}_{i+1}^i \mathbf{n}_{i+1}^{i+1} + \mathbf{P}_{i+1}^i \times \mathbf{f}_i^i \quad (59)$$

The joint actuator torque required to maintain static equilibrium is obtained by taking the vector dot product of the moment vector acting on the link and the joint axis vector.

$$\tau_i = \mathbf{n}_i^{i^T} \mathbf{Z}_i^i \quad (60)$$

b. Manipulator Jacobian in the Force Domain

When an object is displaced through some distance $\delta\chi$ by some force F , work is performed. The same idea holds true for a manipulator arm as it articulates. Allowing the displacement to become infinitesimally small (*principle of virtual work*) and knowing that the amount of work performed is the dot product of a vector force or torque and a vector displacement, the following relationship may be written:

$$F \cdot \delta\chi = \tau \cdot \delta\theta \quad (61)$$

or

$$F^T \delta\chi = \tau^T \delta\theta \quad (62)$$

where F is a 6×1 Cartesian force-moment vector acting at the end-effector, $\delta\chi$ is a 6×1 infinitesimal Cartesian displacement of the end effector, τ is a 6×1 vector of joint torques and $\delta\theta$ is a 6×1 vector of joint displacements. Using the definition of the **Jacobian**

$$\delta\chi = J\delta\theta \quad (63)$$

substituting into Equation (63) and transposing yields

$$\tau = J^T F \quad (64)$$

This result states that the **Jacobian transpose** maps the cartesian forces seen at the end-effector into equivalent

joint torques. The *PUMA Manipulator Jacobian* is developed in Appendix C.

B. IMPLEMENTATION

1. Force Override Rate Controller Algorithm

As seen from the previous section, utilization of the Jacobian transpose as an operator on the force matrix allows us to compute the equivalent joint torque matrix. If the individual joint angles can be read, then the required change in joint angles may be computed from the algorithm in Figure 22, where q is a generalized joint variable accounting for rotary as well as prismatic joints (θ , d) and k is an arbitrary constant to be selected experimentally.

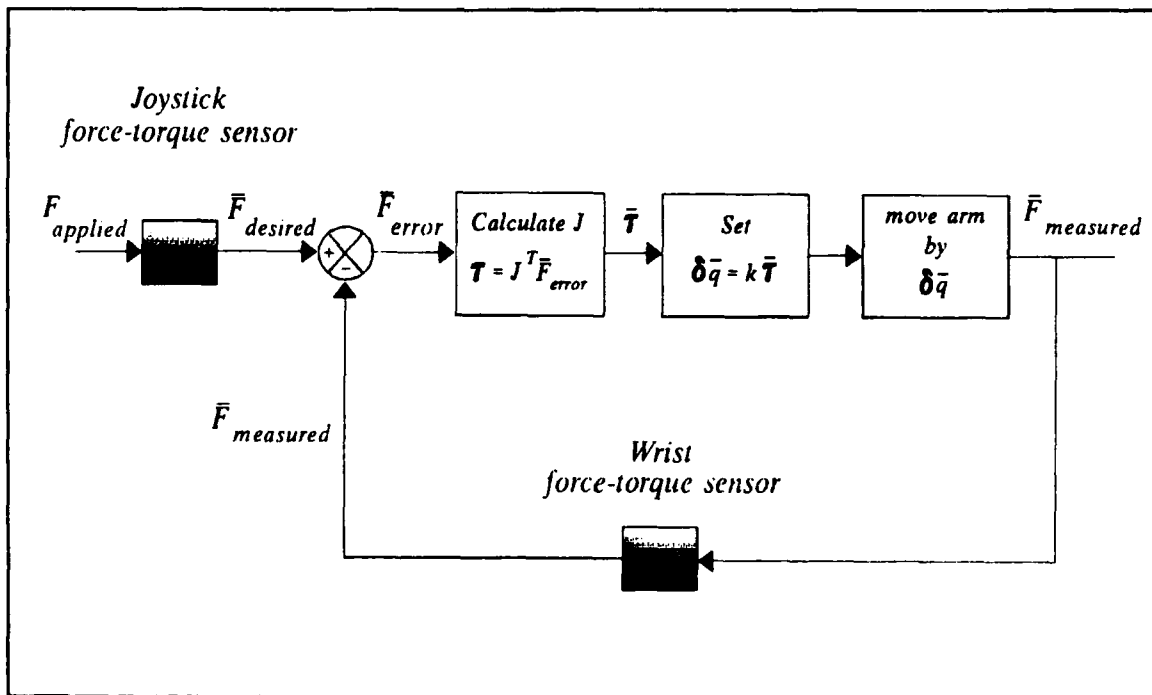


Figure 22. Force Control Algorithm

V. CONCLUSIONS

A. EXPERIMENTAL AND THEORETICAL RESULTS

- Force override rate control works as demonstrated by the single degree of freedom hydraulic actuation system.
- A force-torque transducer may be constructed using force sensing resistors.
- Two examples of transducers have been designed in which a specific pattern of FSR's may be used to measure the desired forces and torques applied to the transducer.
- The method of checking the system coefficient matrix **A** provides a design approach for any order transducer.

B. FURTHER WORK

- Calibrate the current prototype to measure two force and two moment components.
- Investigate the feasibility of sensor redundancy.
- Construct a new reduced order prototype using a larger cube so that individual FSR's do not overlap the ends of the cube.
- Upon successful calibration and testing of prototype, construct a second transducer to be used as a joystick.
- Implement transducers in a controller algorithm for testing using the *PUMA 560*.

APPENDIX A

The following table is based on the sensor placement pattern depicted in Figure 13 and the sensor equations developed in Chapter III.

TABLE 7. 54 SENSOR COEFFICIENT ARRAY

	F_x^+	F_x^-	F_y^+	F_y^-	F_z^+	F_z^-	M_x^+	M_x^-	M_y^+	M_y^-	M_z^+	M_z^-
S_1	19	0	0	0	0	0	0	0	0	3	0	3
S_2	19	0	0	0	0	0	0	0	0	3	0	0
S_3	19	0	0	0	0	0	0	0	0	3	3	0
S_4	4	0	0	0	0	0	0	0	0	0	0	3
S_5	4	0	0	0	0	0	0	0	0	0	0	0
S_6	4	0	0	0	0	0	0	0	0	0	3	0
S_7	0	11	0	0	0	0	0	0	3	0	0	3
S_8	0	11	0	0	0	0	0	0	3	0	0	0
S_9	0	11	0	0	0	0	0	0	3	0	3	0
S_{10}	0	19	0	0	0	0	0	0	3	0	0	3
S_{11}	0	19	0	0	0	0	0	0	3	0	0	0
S_{12}	0	19	0	0	0	0	0	0	3	0	3	0
S_{13}	0	4	0	0	0	0	0	0	0	0	0	3
S_{14}	0	4	0	0	0	0	0	0	0	0	0	0
S_{15}	0	4	0	0	0	0	0	0	0	0	3	0
S_{16}	11	0	0	0	0	0	0	0	0	3	0	3
S_{17}	11	0	0	0	0	0	0	0	0	3	0	0
S_{18}	11	0	0	0	0	0	0	0	0	3	3	0
S_{19}	0	0	19	0	0	0	3	0	0	0	0	3
S_{20}	0	0	19	0	0	0	3	0	0	0	0	0
S_{21}	0	0	19	0	0	0	3	0	0	0	3	0
S_{22}	0	0	4	0	0	0	0	0	0	0	0	3
S_{23}	0	0	4	0	0	0	0	0	0	0	0	0
S_{24}	0	0	4	0	0	0	0	0	0	0	3	0
S_{25}	0	0	0	11	0	0	0	3	0	0	0	3
S_{26}	0	0	0	11	0	0	0	3	0	0	0	0
S_{27}	0	0	0	11	0	0	0	3	0	0	3	0
S_{28}	0	0	0	19	0	0	0	3	0	0	0	3
S_{29}	0	0	0	19	0	0	0	3	0	0	0	0
S_{30}	0	0	0	19	0	0	0	3	0	0	3	0

S_{31}	0	0	0	4	0	0	0	0	0	0	0	3
S_{32}	0	0	0	4	0	0	0	0	0	0	0	0
S_{33}	0	0	0	4	0	0	0	0	0	0	3	0
S_{34}	0	0	11	0	0	0	3	0	0	0	0	3
S_{35}	0	0	11	0	0	0	3	0	0	0	0	0
S_{36}	0	0	11	0	0	0	3	0	0	0	3	0
S_{37}	0	15	15	0	0	4	3	0	3	0	0	0
S_{38}	0	15	0	0	0	4	0	0	3	0	0	0
S_{39}	0	15	0	15	0	4	0	3	3	0	0	0
S_{40}	0	0	15	0	0	4	3	0	0	0	0	0
S_{41}	0	0	0	0	0	4	0	0	0	0	0	0
S_{42}	0	0	0	15	0	4	0	3	0	0	0	0
S_{43}	15	0	15	0	0	4	3	0	0	3	0	0
S_{44}	15	0	0	0	0	4	0	0	0	3	0	0
S_{45}	15	0	0	15	0	4	0	3	0	3	0	0
S_{46}	0	15	0	15	4	0	0	3	3	0	0	0
S_{47}	0	15	0	0	4	0	0	0	3	0	0	0
S_{48}	0	15	15	0	4	0	3	0	3	0	0	0
S_{49}	0	0	0	15	4	0	0	3	0	0	0	0
S_{50}	0	0	0	0	4	0	0	0	0	0	0	0
S_{51}	0	0	15	0	4	0	3	0	0	0	0	0
S_{52}	15	0	0	15	4	0	0	3	0	3	0	0
S_{53}	15	0	0	0	4	0	0	0	0	3	0	0
S_{54}	15	0	15	0	4	0	3	0	0	3	0	0

The full order sensor coefficient matrix is the 54x12 array in Table 7 (rather than the transpose in previous cases). Premultiplying this matrix by its transpose yields a full rank 12x12 matrix, thus verifying that all 12 force-torque components are determinable. Having determined the upper bound for the number of sensors n , and knowing the lower limit to be 12, individual sensors were eliminated in patterns. The procedure is outlined in Table 8.

TABLE 8. SENSOR ELIMINATION STRATEGY

<i>Action</i>	<i>Face</i>	<i>Sensors Remaining</i>	<i>Rank</i>
<i>Eliminate middle rows and columns</i>			
Delete S_2, S_4, S_6, S_8	X ⁺	50	12
Delete S_5	X ⁺	49	12
Delete $S_{11}, S_{13}, S_{14}, S_{15}, S_{17}$	X ⁻	44	12
Delete $S_{20}, S_{22}, S_{23}, S_{24}, S_{26}$	Y ⁺	39	12
Delete $S_{29}, S_{31}, S_{32}, S_{33}, S_{35}$	Y ⁻	34	11
Add S_{32}	Y ⁻	35	11
Add $S_{29}, S_{31}, S_{33}, S_{35}$	Y ⁻	39	12
Delete $S_{38}, S_{40}, S_{41}, S_{42}, S_{44}$	Z ⁻	34	12
Delete $S_{47}, S_{49}, S_{50}, S_{51}, S_{53}$	Z ⁺	29	12
<i>Eliminate diagonals</i>			
Delete S_3, S_7	X ⁺	27	12
Delete S_{10}, S_{18}	X ⁻	25	12
Delete S_{21}, S_{25}	Y ⁺	23	12
Delete S_{39}, S_{43}	Z ⁻	21	12
Delete S_{48}, S_{52}	Z ⁺	19	12
<i>Delete Individual Sensors</i>			
Delete S_{37}	Z ⁻	18	12
Delete S_{45}	Z ⁻	17	11
Add S_{45}	Z ⁻	18	12
Delete S_{46}	Z ⁺	17	12
Delete S_9	X ⁺	16	11
Add S_9	X ⁺	17	12
Delete S_1	X ⁺	16	11
Add S_1	X ⁺	17	12
Delete S_{28}	Y ⁻	16	12
Delete S_{30}	Y ⁻	15	12
Delete S_{34}, S_{36}	Y ⁻	13	12
Delete S_{32}	Y ⁻	12	12

Further elimination of sensors from Table 7 results in a rank deficient coefficient matrix. The full order sensor placement pattern is depicted in Figure 14.

Beginning with a 24x8 coefficient array, for which the rank of $A^T A$ was 8, sensors were selectively eliminated to determine the required placement pattern for the reduced order sensor.

TABLE 9. 24 SENSOR COEFFICIENT ARRAY

	F_x^+	F_x^-	F_y^+	F_y^-	F_z^+	F_z^-	M_z^+	M_z^-
S_1	19	0	0	0	0	0	0	3
S_3	19	0	0	0	0	0	3	0
S_7	0	11	0	0	0	0	0	3
S_9	0	11	0	0	0	0	3	0
S_{10}	0	19	0	0	0	0	0	3
S_{12}	0	19	0	0	0	0	3	0
S_{16}	11	0	0	0	0	0	0	3
S_{18}	11	0	0	0	0	0	3	0
S_{19}	0	0	19	0	0	0	0	3
S_{21}	0	0	19	0	0	0	3	0
S_{25}	0	0	0	11	0	0	0	3
S_{27}	0	0	0	11	0	0	3	0
S_{29}	0	0	0	19	0	0	0	0
S_{31}	0	0	0	4	0	0	0	3
S_{33}	0	0	0	4	0	0	3	0
S_{35}	0	0	11	0	0	0	0	0
S_{37}	0	15	15	0	0	4	0	0
S_{39}	0	15	0	15	0	4	0	0
S_{43}	15	0	15	0	0	4	0	0
S_{45}	15	0	0	15	0	4	0	0
S_{46}	0	15	0	15	4	0	0	0
S_{48}	0	15	15	0	4	0	0	0
S_{52}	15	0	0	15	4	0	0	0
S_{54}	15	0	15	0	4	0	0	0

TABLE 10. SENSOR ELIMINATION STRATEGY

<i>Action</i>	<i>Face</i>	<i>Sensors Remaining</i>	<i>Rank</i>
<i>Eliminate diagonals</i>			
Delete S_3, S_7	X ⁺	22	8
Delete S_{12}, S_{16}	X ⁻	20	8
Delete S_{21}, S_{25}	Y ⁺	18	8
Delete S_{39}, S_{43}	Z ⁻	16	8
Delete S_{48}, S_{52}	Z ⁺	14	8
<i>Eliminate Individual Sensors</i>			
Delete S_{45}	Z ⁻	13	8
Delete S_{54}	Z ⁺	12	8
Delete S_9	X ⁺	11	8
Delete S_{18}	X ⁻	10	8
Delete S_{27}	Y ⁻	9	8
Delete S_{35}	Y ⁻	8	8

Again, further elimination of sensors resulted in a rank deficient coefficient matrix. The individual sensor placement pattern for the reduced order sensor is depicted in Figure 15.

APPENDIX B

Referring to Figure 20 and the link and joint parameters for the PUMA 560 given in Table 6 the individual transformation matrices are computed as follows from Equation (49) [Ref.17]. C_i and S_i are short for $\cos\theta_i$ and $\sin\theta_i$. C_{ij} and S_{ij} are $\cos(\theta_i + \theta_j)$ and $\sin(\theta_i + \theta_j)$ respectively.

$$T_1^0 = \begin{vmatrix} C_1 & 0 & -S_1 & 0 \\ S_1 & 0 & C_1 & 0 \\ 0 & -1 & 0 & 0 \\ 0 & 0 & 0 & 1 \end{vmatrix}$$

$$T_2^1 = \begin{vmatrix} C_2 & -S_2 & 0 & a_2 C_2 \\ S_2 & C_2 & 0 & a_2 S_2 \\ 0 & 0 & 1 & d_2 \\ 0 & 0 & 0 & 1 \end{vmatrix}$$

$$T_3^2 = \begin{vmatrix} C_3 & 0 & S_3 & a_3 C_3 \\ S_3 & 0 & -C_3 & a_3 S_3 \\ 0 & 1 & 0 & 0 \\ 0 & 0 & 0 & 1 \end{vmatrix}$$

$$T_4^3 = \begin{vmatrix} C_4 & 0 & -S_4 & 0 \\ S_4 & 0 & C_4 & 0 \\ 0 & -1 & 0 & d_4 \\ 0 & 0 & 0 & 1 \end{vmatrix}$$

$$T_5^4 = \begin{vmatrix} C_5 & 0 & S_5 & 0 \\ S_5 & 0 & -C_5 & 0 \\ 0 & 1 & 0 & 0 \\ 0 & 0 & 0 & 1 \end{vmatrix}$$

$$T_6^5 = \begin{vmatrix} C_6 & -S_6 & 0 & 0 \\ S_6 & C_6 & 0 & 0 \\ 0 & 0 & 1 & d_6 \\ 0 & 0 & 0 & 1 \end{vmatrix}$$

Multiplying the first and last three transformation matrices together produces the following

$$T_1 \equiv T_1^0 T_2^1 T_3^2 = \begin{vmatrix} C_1 C_{23} & -S_1 & C_1 S_{23} & a_2 C_1 C_2 + a_3 C_1 C_{23} - d_2 S_1 \\ S_1 C_{23} & C_1 & S_1 S_{23} & a_2 S_1 C_2 + a_3 S_1 C_{23} + d_2 C_1 \\ -S_{23} & 0 & C_{23} & -a_2 S_2 - a_3 S_{23} \\ 0 & 0 & 0 & 1 \end{vmatrix}$$

$$T_2 \equiv T_4^3 T_5^4 T_6^5 = \begin{vmatrix} C_4 C_5 C_6 - S_4 S_6 & -C_4 C_5 C_6 - S_4 S_6 & C_4 S_5 & d_6 C_4 S_5 \\ S_4 C_5 C_6 + C_4 S_6 & -S_4 C_5 S_6 + C_4 C_6 & S_4 S_5 & d_6 S_4 S_5 \\ -S_5 C_6 & S_5 S_6 & C_5 & d_6 C_5 + d_4 \\ 0 & 0 & 0 & 1 \end{vmatrix}$$

Multiplying T_1 and T_2 gives the **manipulator arm matrix**

$$T_6^0 = T_3^0 T_6^3 = T_1 T_2 = \begin{vmatrix} I_{11} & I_{12} & I_{13} & P_x \\ I_{21} & I_{22} & I_{23} & P_y \\ I_{31} & I_{32} & I_{33} & P_z \\ 0 & 0 & 0 & 1 \end{vmatrix}$$

$$r_{11} = C_1 [C_{23} (C_4 C_5 C_6 - S_4 S_6) - S_{23} S_5 C_6] - S_1 (S_4 C_5 C_6 + C_4 S_6)$$

$$r_{21} = S_1 [C_{23} (C_4 C_5 C_6 - S_4 S_6) - S_{23} S_5 C_6] + C_1 (S_4 C_5 C_6 + C_4 S_6)$$

$$r_{31} = -S_{23} [C_4 C_5 C_6 - S_4 S_6] - C_{23} S_5 C_6$$

$$r_{12} = S_1 [C_{23} (C_4 C_5 C_6 - S_4 S_6) - S_{23} S_5 C_6] + C_1 (S_4 C_5 C_6 + C_4 S_6)$$

$$r_{22} = S_1 [-C_{23} (C_4 C_5 C_6 + S_4 S_6) + S_{23} S_5 C_6] + C_1 (-S_4 C_5 C_6 + C_4 S_6)$$

$$r_{32} = S_{23} (C_4 C_5 S_6 + S_4 C_6) + C_{23} S_5 S_6$$

$$r_{13} = C_1 (C_{23} C_4 S_5 + S_{23} C_5) - S_1 S_4 S_5$$

$$r_{23} = S_1 (C_{23} C_4 S_5 + S_{23} C_5) - C_1 S_4 S_5$$

$$r_{33} = -S_{23} C_4 S_5 + C_{23} C_5$$

$$p_x = C_1 [d_6 (C_{23} C_4 S_5 + S_{23} C_5) + S_{23} d_4 + a_3 C_{23} + a_2 C_2] - S_1 (d_6 S_4 S_5 + d_2)$$

$$p_y = S_1 [d_6 (C_{23} C_4 S_5 + S_{23} C_5) + S_{23} d_4 + a_3 C_{23} + a_2 C_2] + C_1 (d_6 S_4 S_5 + d_2)$$

$$p_z = d_6 (C_{23} C_5 - S_{23} C_4 S_5) + C_{23} d_4 - a_3 S_{23} - a_2 S_2$$

APPENDIX C

Fu [Ref. 18] derives the **PUMA 560 Manipulator Jacobian** by the *Differential Translation and Rotation Method*. The columns of this 6x6 matrix are as follows:

$$J_1(\theta) = \begin{bmatrix} J_{1x} \\ J_{1y} \\ J_{1z} \\ -[S_{23}(C_4C_5C_6 - S_4S_6) + C_{23}S_5C_6] \\ S_{23}(C_4C_5S_6 + S_4C_6) + C_{23}S_5S_6 \\ -S_{23}C_4S_5 + C_{23}C_5 \end{bmatrix}$$

where

$$\begin{aligned} J_{1x} &= [d_6(C_{23}C_4S_5 + S_{23}C_5) + d_4S_{23} + a_3C_{23} + a_2C_2](S_4C_5C_6 + C_4S_6) \\ &\quad - (d_6S_4S_5 + d_2)[C_{23}(C_4C_5C_6 - S_4S_6) - S_{23}S_5C_6] \\ J_{1y} &= [d_6(C_{23}C_4S_5 + S_{23}C_5) + d_4S_{23} + a_3C_{23} + a_2C_2](-S_4C_5S_6 + C_4C_6) \\ &\quad - (d_6S_4S_5 + d_2)[-C_{23}(C_4C_5S_6 + S_4C_6) + S_{23}S_5S_6] \\ J_{1z} &= [d_6(C_{23}C_4S_5 + S_{23}C_5) + d_4S_{23} + a_3C_{23} + a_2C_2](S_4S_5) \\ &\quad - (d_6S_4S_5 + d_2)(C_{23}C_4S_5 + S_{23}C_5) \end{aligned}$$

$$J_2(\theta) = \begin{bmatrix} J_{2x} \\ J_{2y} \\ J_{2z} \\ S_4C_5C_6 + C_4S_6 \\ -S_4C_5S_6 + C_4S_6 \\ S_4S_5 \end{bmatrix}$$

where

$$J_{2x} = (d_6S_3C_5 + d_6C_3C_4S_5 + d_4S_3 + a_3C_3 + a_2)(S_5C_6)$$

$$\begin{aligned}
& -(-d_6 C_3 C_5 + d_6 S_3 C_4 S_5 - d_4 C_3 + a_3 S_3) (C_4 C_5 C_6 - S_4 S_6) \\
J_{2y} = & -(d_6 S_3 C_5 + d_6 C_3 C_4 S_5 + d_4 S_3 + a_3 C_3 + a_2) (S_5 S_6) \\
& + (-d_6 C_3 C_5 + d_6 S_3 C_4 S_5 - d_4 C_3 + a_3 S_3) (C_4 S_5) \\
J_{2z} = & -(d_6 S_3 C_5 + d_6 C_3 C_4 S_5 + d_4 S_3 + a_3 C_3 + a_2) C_5 \\
& -(-d_6 C_3 C_5 + d_6 S_3 C_4 S_5 - d_4 C_3 + a_3 S_3) (C_4 S_5)
\end{aligned}$$

$$J_3(\theta) = \begin{vmatrix} (a_3 + d_6 C_4 S_5) (S_5 C_6) + (d_4 + d_6 C_5) (C_4 C_5 C_6 - S_4 S_6) \\ -(a_3 + d_6 C_4 S_5) (S_5 S_6) - (d_4 + d_6 C_5) (C_4 C_5 C_6 + S_4 S_6) \\ -(a_3 + d_6 C_4 S_5) C_5 + (d_4 + d_6 C_5) C_4 S_5 \\ S_4 C_5 C_6 + C_4 S_6 \\ -S_4 C_5 S_6 + C_4 S_6 \\ S_4 S_5 \end{vmatrix}$$

$$J_4(\theta) = \begin{vmatrix} d_6 S_5 S_6 \\ d_6 S_5 C_6 \\ 0 \\ -S_5 C_6 \\ S_5 S_6 \\ C_5 \end{vmatrix}$$

$$J_5(\theta) = \begin{vmatrix} d_6 C_6 \\ -d_6 S_6 \\ 0 \\ S_6 \\ C_6 \\ 0 \end{vmatrix}$$

$$J_6(\theta) = \begin{vmatrix} 0 \\ 0 \\ 0 \\ 0 \\ 0 \\ 1 \end{vmatrix}$$

LIST OF REFERENCES

1. Craig, John J., *Introduction to Robotics, Second Edition*, p. 383, Addison-Wesley Publishing Company, Inc., 1989.
2. Fu, K.S., Gonzalez, R.C., and Lee, C.S.G., *Robotics: Control, Sensing, Vision, and Intelligence*, p. 290, McGraw-Hill Book Company, 1987.
3. Fu, K.S., Gonzalez, R.C., and Lee, C.S.G., *Robotics: Control, Sensing, Vision, and Intelligence*, pp. 289-293, McGraw-Hill Book Company, 1987.
4. *Force and Position Sensing Resistors*, Interlink Electronics, Revision 2/90.
5. Craig, John J., *Introduction to Robotics, Second Edition*, p. 21, Addison-Wesley Publishing Company, Inc., 1989.
6. Craig, John J., *Introduction to Robotics, Second Edition*, p. 23, Addison-Wesley Publishing Company, Inc., 1989.
7. Craig, John J., *Introduction to Robotics, Second Edition*, p. 23, Addison-Wesley Publishing Company, Inc., 1989.
8. Craig, John J., *Introduction to Robotics, Second Edition*, p. 38, Addison-Wesley Publishing Company, Inc., 1989.
9. Fu, K.S., Gonzalez, R.C., and Lee, C.S.G., *Robotics: Control, Sensing, Vision, and Intelligence*, p. 36, McGraw-Hill Book Company, 1987.
10. Fu, K.S., Gonzalez, R.C., and Lee, C.S.G., *Robotics: Control, Sensing, Vision, and Intelligence*, p. 35, McGraw-Hill Book Company, 1987.
11. Fu, K.S., Gonzalez, R.C., and Lee, C.S.G., *Robotics: Control, Sensing, Vision, and Intelligence*, p. 37, McGraw-Hill Book Company, 1987.
12. Fu, K.S., Gonzalez, R.C., and Lee, C.S.G., *Robotics: Control, Sensing, Vision, and Intelligence*, p. 40, McGraw-Hill Book Company, 1987.
13. Fu, K.S., Gonzalez, R.C., and Lee, C.S.G., *Robotics: Control, Sensing, Vision, and Intelligence*, p. 37, McGraw-Hill Book Company, 1987.

14. Fu, K.S., Gonzalez, R.C., and Lee, C.S.G., *Robotics: Control, Sensing, Vision, and Intelligence*, p. 53, McGraw-Hill Book Company, 1987.
15. Craig, John J., *Introduction to Robotics, Second Edition*, pp. 131-136, Addison-Wesley Publishing Company, Inc., 1989.
16. Craig, John J., *Introduction to Robotics, Second Edition*, pp. 175-182, Addison-Wesley Publishing Company, Inc., 1989.
17. Fu, K.S., Gonzalez, R.C., and Lee, C.S.G., *Robotics: Control, Sensing, Vision, and Intelligence*, pp. 41-45, McGraw-Hill Book Company, 1987.
18. Fu, K.S., Gonzalez, R.C., and Lee, C.S.G., *Robotics: Control, Sensing, Vision, and Intelligence*, pp. 547-553, McGraw-Hill Book Company, 1987.

INITIAL DISTRIBUTION LIST

	<u>No. Copies</u>
1. Defense Technical Information Center Cameron Station Alexandria, Virginia 22304-6145	2
2. Mr. Jim Moore New Initiatives Office NASA Johnson Space Center 2101 NASA Road 1 Houston, Texas 77058-3691	1
3. Mr. L. Monford NASA Johnson Space Center Mail Stop ER Houston, Texas 77058	1
4. Naval Engineering Curricular Office Code 34 Department of Mechanical Engineering Naval Postgraduate School Monterey, California 93943-5000	1
5. Library, Code 052 Naval Postgraduate School Monterey, California 93943-5002	2
6. Department Chairman, Code ME Department of Mechanical Engineering Naval Postgraduate School Monterey, California 93943-5000	1
7. Professor Morris Driels, Code ME/Dr Department of Mechanical Engineering Naval Postgraduate School Monterey, California 93943-5000	3
8. LT James M. Syvertsen 20 Leonard Street Wading River, New York 11792	3